Antisolvent Gibbsite Crystallisation from Synthetic Bayer Liquor

University of Cape Town

Yu-Lun Chiang

Supervisors: Prof Alison Lewis & Mr Jeeten Nathoo

A dissertation submitted for the degree of Master of Science in Engineering in Chemical Engineering

2009

DECLARATIONS

(i) I hereby grant the University of Cape Town free licence to reproduce for the purpose of research either the whole or any portion of the contents in any manner whatsoever of the above dissertation. I am presenting this dissertation in **COMPLETE / PARTIAL** fulfilment of the requirements for my degree.

(ii) I know the meaning of plagiarism and declare that all of the work in the document, save for that which is properly acknowledged, is my own.

Mr Yu-Lun Chiang

Executive Summary

The current Bayer precipitation of gibbsite is notoriously slow and is considered to be the rate limiting step of the Bayer process. The present industrial reactor configuration involves precipitating gibbsite inside a series of large stainless steel agitated vessels due to the slow precipitation kinetics of gibbsite from pregnant Bayer liquor.

The scope of this study is to investigate the effectiveness of using water as an antisolvent to increase the overall gibbsite yield and the associated particle behaviours under isothermal conditions.

The experiments were performed in a series of batch experiments which were divided into two subsets. Firstly, the effect of different caustic concentrations present in the antisolvent on gibbsite yield was tested. Secondly, the effect of different seed loading (50 and 100 grams seeds per liter of synthetic liquor) on aggregation and fines formation were investigated. All batch experiments were conducted isothermally at 80°C under a closed system using a baffled stainless steel 316 agitated vessel.

The experimental results indicated water to be a feasible medium for the isothermal antisolvent crystallisation of gibbsite from synthetic pregnant Bayer liquor. It was found that the extent of overall gibbsite yield exhibits a power law correlation to the change in the antisolvent caustic concentration with $R^2 \approx 1$ ($R^2 = 0.99974$). This finding is important as the regressed curve will be used to correlate gibbsite yield as a function of antisolvent purity.

From the seed loading experiments, an increase in seed loading under constant temperature and initial liquor supersaturation resulted in an overall decrease in product particle size due to a rise in inter-particulate attrition. However, crystal growth was not dominant during any period of the experiments with aggregation being more prominent for the system with the lower seed load. Gibbsite morphology determination from SEM revealed hexagonal solids which, in the presence of a higher seed loading indicated signs of fracture due to attrition.

Quantitative evidence of this mechanism is shown using the discretised population balance method by Bramley et al. (1996) with the aid of the computational technique

developed by Hounslow (2005) in Mathematica. Results generated using this method show decreasing aggregation with liquor desupersaturation and increased seed loading.

The overall particle behaviours from the current investigation are validated by results obtained from previous gibbsite studies under very similar conditions. Although the gibbsite yield can be increased drastically in the presence of an antisolvent, the average particle size generated from this study is still too small to be commercially feasible due to the increase in initial supersaturation. Thus it is recommended that further particle size optimisation may be conducted inside a fluidised bed reactor where particles generally experience lower shear than inside a conventional agitated vessel.

Acknowledgement

Firstly, I would like to express my sincere appreciation and gratitude to Professor Alison Lewis for granting me the opportunity to undertake a challenging and rewarding project, and for always inspiring me with in-depth guidance and encouragement especially when the going gets tough. Her assistance in finding an external examiner and in the compilation of the dissertation is also gratefully appreciated.

Secondly, I would also like to express my sincere appreciation to Mr Jeeten Nathoo for his constant guidance both in and out of the lab. He has been available as my tutor, mentor, supervisor and a friend from whom he is always keen to offer his experience, advice and encouragement throughout my student career at UCT. His calm approach in dealing with tough problems always makes him a pleasure to work with.

Big thanks must also go to Mrs Helen Divey for her expert advice and assistance on the Malvern Mastersizer, the ultrasound and performing the AAS. She is always willing to offer advice on any queries regarding the laboratory and waste disposal. Thank you!

Many thanks must also go to Ms Miranda Waldron from the Department of Physics for her help on the SEM and EDAX; to Ms Ronel August from the Department of Geological Sciences for supervising my initial startup of the XRD unit for analysis; and to Dr Chris Vernon, Dr Tian Li and Prof Mike Hounslow for their expert advice during my study.

I would also like to thank Mr David Bramble for his work on the construction of the reaction vessels and all the associated ancillaries.

My appreciation is also extended to my former and current colleagues from the Crystallisation and Precipitation Unit for their support and encouragements, and to Mrs Christine Olsen for always making our research administration a pleasurable experience.

To my parents, thank you for your inspiration and giving me much needed moral support throughout my academic career.

Last but not least, I would like to extend my appreciation to the NRF, THRIP and ALCOA for providing the necessary funding for this project to commence.

Table of Contents

List of Figures

List of Tables

1. Introduction

1.1 Industrial background

Crystallisation and precipitation reactions are widely utilized in the food, pharmaceutical and mineral processing industries. Some examples are the production of Aspirin, effervescent supplement tablets and industrial diamonds. Although these substances and industries may seem to differ vastly, the underlying fundamentals they possess are the same.

The thesis begins with a section on how precipitate characteristics may be manipulated by gaining some understanding into some fundamental parameters which govern the precipitation processes. The ways in which these fundamentals are put into practice for the current field of study will then be applied.

1.2 Process background

The Bayer Process currently governs the upstream processing of anhydrous alumina in preparation for its electrolytic conversion into aluminium metal. Bauxite ore is crushed and digested in hot caustic soda before the Pregnant Bayer Liquor (PBL) is purified of any undigested gangue and other impurities. The clear PBL is then extracted by removing the impurities via thickening and filtration. Gibbsite (a hydrated polymorph of alumina) is then re-crystallised out of solution by evaporative cooling and routed to a furnace where a dehydration process transforms the gibbsite into anhydrous alumina. The dried product is then converted into aluminum metal via electrowinning. A simplified block diagram of the Bayer Process is presented in Figure 1.

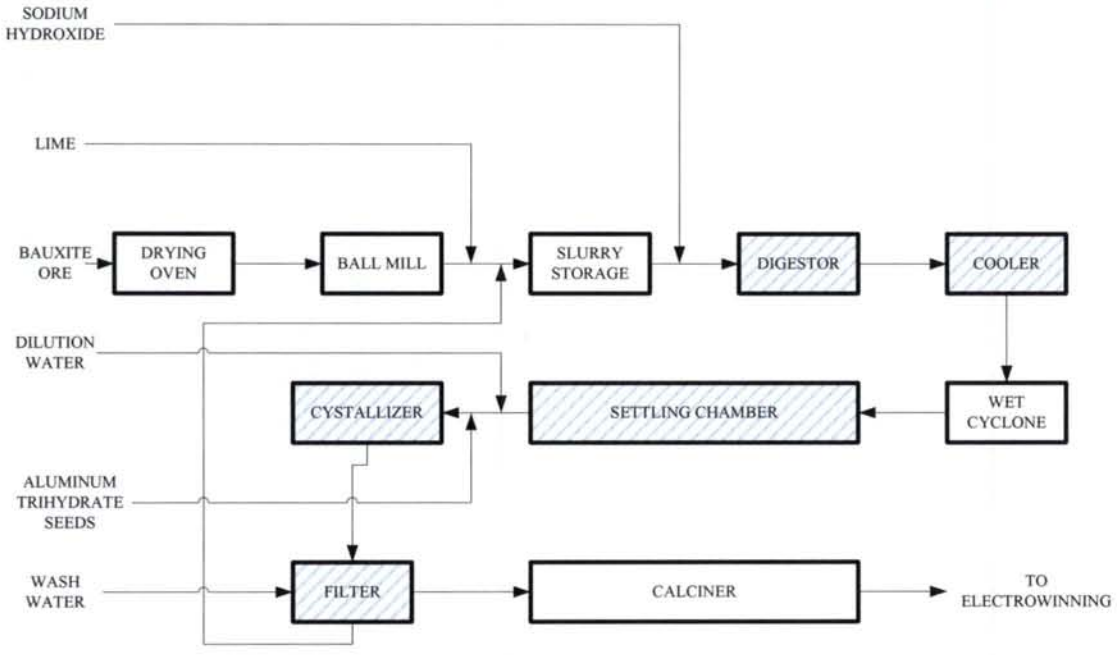

Figure 1: A simplified diagram of the Bayer Process (Pacific Environmental Services Inc., 1998).

The use of an antisolvent to re-crystallise gibbsite from PBL has the potential to positively influence the operation of the Bayer Process. This is especially true if the antisolvent can be easily recovered after the re-crystallisation step. Also known as "drowning-out" crystallisation, an antisolvent reduces the solubility of a particular solute in solution, thus promoting crystallisation of that solute. Antisolvents are already used industrially to recover solid products from solution.

The use of water as an antisolvent to recover gibbsite is based on the overall equilibrium relationship that exists within the Bayer liquor (Geniesse et al., 2007, Ilievski, 1991):

$$Al(OH)_3 + NaOH \leftrightarrow NaAl(OH)_4 \leftrightarrow NaAlO_2 + 2H_2O \qquad (1)$$

The addition of water shifts the above equilibrium to the left, forcing the re-generation of sodium hydroxide (Geniesse et al., 2007) and the gibbsite product. Since water is currently used as a blending agent to adjust the a/c (alumina/caustic) ratio of the pregnant Bayer liquor, no additional reagents and unit operations are required. It is non-toxic and could be removed by evaporation or other methods. The current spent liquor recycle stream undergoes evaporation to increase its caustic concentration (Pacific Environmental Services, Inc. 1998).

However, water addition is currently not a commercially viable process for a Bayer plant as it uses a closed circuit, and the cost of evaporating more water is not justified by the increased yield. Nonetheless, the objective of this study is to investigate the extent of gibbsite product yield from supersaturated Bayer liquors in the presence of an antisolvent and the particle behaviour that is associated with this addition.

1.3 Aim of study

The aim of the study is to:

1 Perform a preliminary feasibility analysis on the effectiveness of water as an antisolvent on gibbsite precipitation.
2 Investigate the effect of antisolvent addition on aggregation, fines formation and gibbsite product quality in the presence of seeding.

1.4 Project objectives

1 To determine the conversion time of a base case Bayer gibbsite precipitation in the absence of an antisolvent.
2 To determine the conversion time in the presence of pure water as an antisolvent.
3 To investigate the effect of caustic concentration on the effect of the antisolvent on the yield of gibbsite.
4 To investigate the effects of different seed loadings on product fines formation.

These objectives are carried out in a set of batch experiments conducted isothermally at 80°C.

2. General Precipitation Theory

2.1 Supersaturation

Supersaturation is the thermodynamic driving force of a crystallization process. It is often defined as the difference in chemical potential of a solution between its current and its equilibrium state – this can also be defined using a variable such as solute concentration. The relationship is shown below (4 Myerson, 2002):

$$\frac{\mu - \mu_{sat}}{R \cdot T} = \ln\left(\frac{a}{a_{sat}}\right) = \ln\left(\frac{\gamma \cdot c}{\gamma_{sat} \cdot c_{sat}}\right) \qquad (2)$$

This is the fundamental expression for quantifying supersaturation in dimensionless form, where μ is the solution chemical potential in J/mol, c is the solution concentration in mol/dm^3, a is the activity, γ is the activity coefficient and the subscripted sat defines the saturation / equilibrium values of these parameters. According to Myerson (2002), simplification of Equation 2 can be carried out should one assume a γ/γ_{sat} ratio of approximately 1, leaving the concentration terms. However, the author also stresses the poor accuracy of the above assumption, but it is nevertheless still used since thermodynamic data are usually unavailable (Myerson, 2002) Equation 2 can now be related as follows (Karbanee, 2007)

$$\ln\left(\frac{\gamma \cdot c}{\gamma_{sat} \cdot c_{sat}}\right) = \ln\left(\frac{c}{c_{sat}}\right) = \frac{c}{c_{sat}} - 1 = S - 1 = \sigma \qquad (3)$$

In Equation 3 S is the relative supersaturation ratio and σ quantifies the absolute supersaturation.

As the most important parameter for crystallisation processes, supersaturation determines the types of mechanisms a crystallisation process will undergo. The principle mechanisms are listed below (Löffelmann, 2002):

- Primary (homogeneous or heterogeneous) and secondary nucleation,
- crystal growth,
- aggregation, and
- attrition

Supersaturation is a function of several parameters such as temperature, pressure, solubility and concentration.

The degree of supersaturation across a range of reaction systems is a function of the solubility product (K_{sp}) of the solute or the precipitate in the solvent. Using the analogy in Myerson (2002) and taking a readily water soluble metal halide such as silver chloride (AgCl), the dissociation reaction in water is shown:

$$AgCl_{(s)} \leftrightarrow Ag^{+} + Cl^{-} \tag{4}$$

The expression for the equilibrium constant K can be written in standard form in terms of the activity of the halide and its ions:

$$K = (a_{Ag}{}^{+}a_{Cl}{}^{-})/(a_{AgCl}) \tag{5}$$

Since AgCl is a stable under standard temperature and pressure (STP), its activity may be equated to 1. This resulted in the simplification of Equation 5 to the following form:

$$K_{sp} = a_{Ag}{}^{+}a_{Cl}{}^{-} = \gamma_{Ag}{}^{+}c_{Ag}{}^{+}\gamma_{Cl}{}^{-}c_{Cl}{}^{-} = c_{Ag}{}^{+}c_{Cl}{}^{-} \tag{6}$$

Myerson made the assumption that for sparingly soluble species, their corresponding activity coefficients may also be set to 1. This leaves the solubility products K_{sp} as a function of only the equilibrium ionic species in the aqueous solution. Equation 6 can thus be related to Equation 3 for relative supersaturation ratio S:

$$S = \frac{c}{c_{sat}} = \frac{c}{K_{sp}} \tag{7}$$

According to Equation 7, the relative supersaturation ratio S of a solution is inversely proportional to the solubility product of the solute in that solution. For example, the degree of supersaturation of aluminum hydroxide ($Al(OH)_3$) will be much higher than barium nitrate ($Ba(NO_3)_2$), since the K_{sp} for $Al(OH)_3$ is 3.70×10^{-15} compared to that obtained for $Ba(NO_3)_2$ of 4.64×10^{-3}.

2.2 Metastability and induction time

The phenomenon of metastability is closely related to the supersaturation property of the solution. It can be defined as a period where a solution's Gibbs free energy reaches a

local minimum. This time is often termed the width of the metastable zone. The width of a metastable zone differs from solution to solution since it is also a strong function of the solubility product of the solute. Table 1 gives some examples of metastable width for different solutes for a cooling system.

Table 1: Metastable zone widths for a cooling rate of 5 K/h (A. Mersmann, 1998)

Solute	Metastable zone width (K)
Ammonium alum	3.0
Sodium sulphate	0.3
Boric acid	1.9

Graphically, the metastable zone can be defined as the region that lies between the solution saturation line and the boundary of the metastable limit across a range of solution temperatures and solute concentrations. The metastable limit is a threshold boundary beyond which spontaneous precipitation will occur with negligible induction time. Figure 2 indicates the position of the metastable zone for a generic solution.

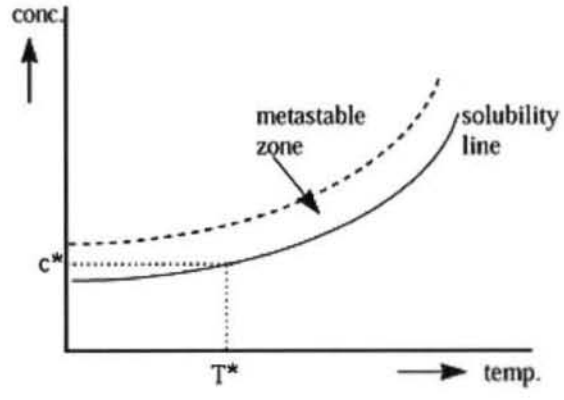

Figure 2: A generic solubility diagram defining the metastable zone (Giulietti, 2001)

The induction time for any precipitation processes can be described as a period where there is no observable change in the solution supersaturation or solid content. From the literature obtained from Ilievski (Ilievski, 1991), the production rate from an industrial crystallizer can be improved by reducing the precipitation induction time. This can be done by manipulating the following parameters:

- increase the supersaturation of the solution – either by evaporation or by antisolvent dilution;
- increase the total seed surface area – either by introducing finer seeds or by increasing the seed loading using existing seeds;
- increase the system temperature.

It is important to keep in mind that induction time is a parameter used to quantify the rate at which a metastable solution equilibrates from a region within the metastable zone towards the solution saturation line.

However, Ilievski (1991) stated that the induction time during the industrial crystallisation of gibbsite from pregnant Bayer liquor is negligible in the presence of seeding and thus ignored.

2.3 Nucleation

Since the metastable property of a supersaturated solution suggests that it is not in a state of equilibrium, it will move towards its saturated state where it will be in a state of lower chemical potential and relieve its supersaturation by crystallisation. Nucleation occurs as a primary crystallisation mechanism in supersaturated homogeneous solutions. This is often followed by more nucleation and crystal growth. Nucleation from supersaturated solution is not spontaneous if the concentration of the solute in the solvent at a specific temperature falls within the corresponding metastable zone. Spontaneous nucleation only occurs at or above the metastable limit as indicated in Figure 2.

When a foreign substance is present, the dominant mechanism is often termed heterogeneous nucleation. In a text written by Volmer (1939), a relationship between the change in free energy of a homogeneous and a heterogeneous system was found. It stated that a decrease in free energy is dependent on the contact angle of the solid phase with the liquid phase. This is quantified by the following equations:

$$\Delta G_{hom} = \phi \cdot \Delta G_{het} \tag{8}$$

$$\phi = \frac{1}{4} \cdot (2 + \cos\theta) \cdot (1 - \cos\theta)^2 \tag{9}$$

In Equation 8 and Equation 9, ΔG_{hom} and ΔG_{het} are defined as the change in Gibbs free energy and ϕ is the surface tension factor as a function of the contact angle θ. The corresponding values calculated for every value of ΔG_{hom} obtained will always be more negative (since ϕ will always be positive for θ ranging from 0° to 360°), thus heterogeneous nucleation will occur more spontaneously than homogeneous nucleation from an identical solution.

If seeds are added in the form of parent crystals, then secondary nucleation may be promoted. According to Myerson (2002), several theories concerning secondary nucleation were proposed. These can be divided into two main categories – the secondary nuclei may originate either from the actual seed crystals or from a boundary layer near the crystals. The author further sub-divided the former into three sources, namely:

- initial or dust breeding;
- needle breeding and,
- collision breeding.

Initial breeding commences when tiny crystallites forms on the surface of the parent seeds during crystal growth. These crystallites may break off from the parent and promote secondary nucleation.

The latter was divided into two sources, namely:

- impurity concentration gradient nucleation and,
- nucleation due to fluid shear.

2.4 Mixing

Since the formation of crystalline products are often achieved by precipitation or antisolvents, the effect of solution mixing is significant in terms of the product particle characterisation. Whether the system is precipitation or crystallisation, the degree of supersaturation is always the highest within a vessel at the point of entry of the reactant

or the antisolvent due to significant concentration differences. The distribution of supersaturation within a reaction system is thus dependent on the scale of fluid mixing.

There are two main scales of mixing that are important in precipitation and crystallisation processes, these are macromixing and micromixing. Macromixing is characterised by fluid flow patterns and turbulent fluid transport, whereas micromixing is mainly a function of molecular interactions and its transport processes. David and Klein (2001) described macromixing as the process contributing to the uniformity of the local average value of the concentrations of all the species present in the vessel. A text from Davidson (1985) describes the dependency of mixing scales on various flow regimes to be related to the rate of reaction of a particular process. This relationship shows that the importance of micro scale mixing becomes more significant when the corresponding rate of reaction increases.

2.5 Antisolvent crystallisation

2.5.1 Purpose

The main techniques currently conducted for crystallisation processes generally revolve around the manipulation of the solution supersaturation by evaporation and cooling.

In an article by Pina et al (2001), the author describe antisolvent crystallisation as a method where the supersaturation of a solution can be generated by adding specific solvents to the initial solution in order to reduce the solubility of the solute. These solvents can either be in solid, liquid or gaseous form. Figure 3 indicates how the use of an antisolvent relates to the other methods of precipitation (Giuletti, 2001):

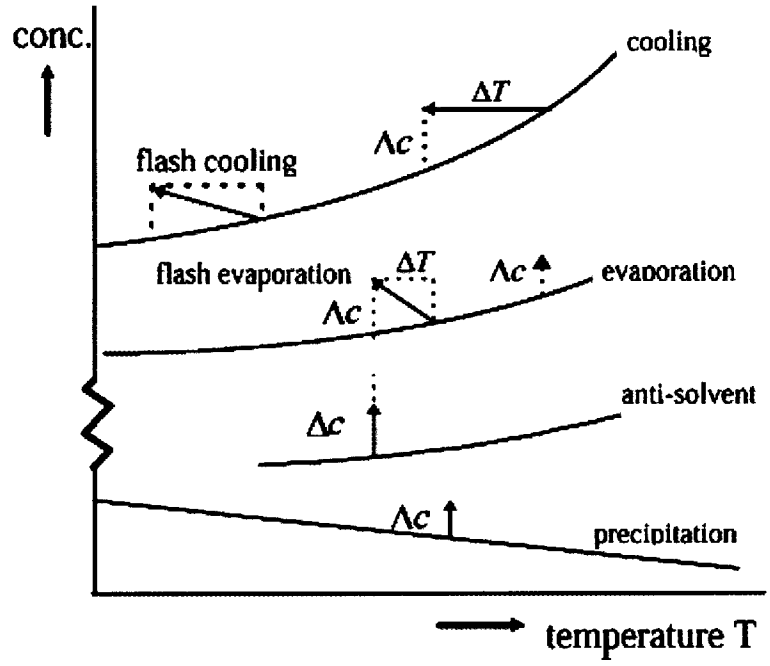

Figure 3: Generic saturation curves showing supersaturation generation from various techniques (Giuletti, 2001)

According to Figure 3, it is evident that antisolvent crystallisation and precipitation are the only two processes where the degree of supersaturation can be increased isothermally. Zijlema et al. (2000) conducted an investigation into the antisolvent crystallisation of sodium chloride (NaCl) as an alternative to the standard evaporative approach. The author stated that the process energy reduction due to the reduction / elimination of the heating and cooling requirements reached as high as 63% when appropriate antisolvents were used as their substitutes.

2.5.2 Generic mechanisms

The exact mechanisms of antisolvent crystallisation are not yet fully understood. However, it is possible to extract the essence of antisolvent behaviours by reviewing papers on various processes under discussion. Mechanism of hydrophilic substitution was briefly mentioned in the article by Zijlema (2000) where antisolvent crystallisation of NaCl using diisopropylamine (DiPA) was investigated at a low temperature. The author discussed how the addition of DiPA as an antisolvent changes the ionic interactions between the solute and the solvent ions. The hydrophilic nature of DiPA towards the water molecules becomes dominant with a decrease in system temperature. This results in

a hydrophilic substitution of DiPA over both the sodium and chloride ions onto the water molecule.

In general, a water-based substance may be used to promote antisolvent crystallisation if the precipitating product is hydrophobic, and alcohol or other organic solvents may be used if the precipitate is hydrophilic (Yeo et al., 2004).

2.5.3 Kinetic aspects

The determination of crystallisation kinetics in the presence of an antisolvent has not yet being investigated extensively. The most appropriate literature currently cited is from Nowee et. al. (2008). From their journal, the authors made reference to Mydlarz and Jones (1989) where crystallisation data were analysed rigorously from 130 experiments to produce a power law model that describes the overall crystal growth relatively well.

3. Gibbsite Precipitation Chemistry

3.1 Solution thermodynamics

The industrial digestion of bauxite ore in hot caustic soda produces a viscous supersaturated solution known as the pregnant Bayer liquor. Since the scope of this study will deal only with synthetic liquors, the effects of organic impurities and other inorganic salts are ignored.

The liquor usually contains aluminate anion complexes that are stabilized by sodium cations (Geniesse et al., 2007). Laboratory synthesis of such liquor often involves high temperature dissolution of hydrated alumina into a concentrated aqueous solution of sodium hydroxide. Ilievski (1991) described the above dissolution process as an overall equilibrium reaction:

$$Al(OH)_{3(s)} + NaOH_{(aq)} \leftrightarrow NaAlO_{2(aq)} + 2H_2O_{(l)} \qquad (10)$$

Ilievski (1991) stressed that the above equilibrium relationship is the result of a series of complex polymerisation steps. The mechanisms of these reaction steps are not yet fully understood.

A recent paper was written on an investigation into the structure of Bayer liquor using spectroscopy and MD simulation (Chen et al., 2006). The results indicated that there exist two dominant aluminate complexes – the monomeric $Al(OH)^{4-}$ ions are found to be dominant in low to medium caustic solutions (< 6 M NaOH) while $Al(OH)_6^{3-}$ ions are dominant in concentrated solutions (> 6 M NaOH). However, it should be kept in mind that the investigators performed the above simulations whilst ignoring the effect of aluminate ion bonding due to lack of information.

The above findings are further consolidated by a more recent paper by Ma et al. (2007) on the structure of sodium aluminate solutions measured using UV spectra. The results from their experiments show the formation of tetrahedral $Al(OH)^{4-}$ when the aluminium concentration is below 1.5 mol/L. Gradual transformation of these tetrahedral anions into $Al_2O(OH)_6^{2-}$ by dehydration were observed as the concentration was increased to 6 mol/L.

However, a number of literature sources (Chen et al. 2006, Counter et al., 1999, Li et al. 2003, Rossiter et al. 1998) all state that the tetrahydrated anions of alumina are the dominant species under Bayer caustic concentrations.

3.2 Gibbsite solubility

Solubility studies on the gibbsite-caustic system were reviewed by Misra (1970) and the following solubility correlation was developed using various gibbsite solubility data:

$$\ln(R) = 6.211 - \frac{2486.7}{(273 + T)} + \frac{1.09c}{(273 + T)} \tag{11}$$

Where: T = liquor temperature (°C)

c = caustic concentration in the liquor in (g/L of Na_2O)

R = ratio of anhydrous alumina-to-caustic in the liquor (A/C)

Ilievski (1991) reported the above correlation to be feasible for a temperature ranging from 25°C to 100°C, and caustic concentrations over the range 30 – 320 g/L disodium oxide (Na_2O). R is the equilibrium ratio of anhydrous alumina (Al_2O_3) to Na_2O often abbreviated as A/C in most literature, and T is the temperature in °C. The author then discussed the correlation of the crystal growth rate G to the solution supersaturation S and its caustic concentration c as follows:

$$G \propto \frac{S^2}{\sqrt{c}} \tag{12}$$

The absolute supersaturation S of the Bayer Liquor from Equation 12 is defined as a function of the operating A/C ratio and the equilibrium A/C ratio R shown below:

$$S = \left(\frac{a}{c} - R\right) \tag{13}$$

However, Rosenberg and Healy (1996) have proposed a more versatile model for gibbsite solubility in Bayer liquors. The proposed model is applicable for both pure and carbonated liquors.

$$A_{eqm} = 0.96197 \cdot C \cdot \left[1 + \frac{10^{\left[\frac{-9.2082 \cdot \sqrt{I}}{(1+\sqrt{I})} + 0.8743 \cdot I - 0.2149 \cdot I^{\frac{3}{2}} \right]}}{\exp\left(\frac{\Delta G}{R \cdot T} \right)} \right]^{-1} \quad (14)$$

The correlation shown in Equation 14 gives a good estimation for equilibrium alumina concentration A_{eqm} in g/L as a function of caustic concentration (g/L), precipitation temperature (in K) and ionic strength I (in g/L of Na_2CO_3). The constants R and ΔG are the universal gas constant and the Gibbs free energy of solid formation (-30.96 kJ/mol). The ionic strength term in Equation 14 is a function of the total alkali metal content present in the liquor. For the case where sodium is the only alkali metal present, Rosenberg and Healy (1996) developed the following correlation:

$$I = 0.01887 \cdot C + 0.01911 \cdot SC \quad (15)$$

Where C and SC are the caustic and carbonate concentrations respectively, both in g/L of Na_2CO_3.

3.3 Polymorphism of alumina hydrate

Three groups of aluminum hydroxides have been discussed by Ilievski (1991), namely bayerite, gibbsite and boehmite. The former two are trihydroxide polymorphs while the third is a monohydrate. The conditions for the formation of these solids all occur at Bayer refinery conditions.

Ilievski also mentioned from several publications that the polymorph transformation of bayerite to gibbsite is temperature and pH dependent. At a liquor pH greater than 12, rapid transformation from bayerite to gibbsite occurs at a precipitation temperatures above 30°C. Past XRD results of alumina hydrate precipitated from Bayer liquor at 80°C have indicated gibbsite to be the only polymorph present (Sakamoto, 1963).

However, previous precipitation investigations using a temperature range between 30°C and 50°C suggested that the formation of the precipitate contains a mixture of bayerite and gibbsite. Ilievski (1991) also referred to several publications where it was found that bayerite eventually transformed to gibbsite at lower temperature ranges (30°C to 50°C).

3.4 Effect of operating temperature

Since the operating temperature of the Bayer crystalliser must be between 60°C and 90°C to initiate the precipitation of gibbsite as the desired polymorph, the exact temperature must be determined to satisfy the scope of the current study. Ilievski referred to White and Bateman (1988) who derived the following correlation for the growth rate G (μm/hr) of gibbsite as a function of caustic concentration c (g/L of Na_2O), temperature T (in K) and absolute supersaturation S:

$$G = \frac{15}{\sqrt{\frac{c}{100}}} \cdot \exp\left[-7600 \cdot \left(\frac{1}{T+273} - \frac{1}{343.16}\right)\right] \cdot S^2 \qquad (16)$$

However, Equation 16 is also a function of Equation 11 and Equation13 and hence the constraint on the temperature and caustic concentration variables applies. Using Equation 16, growth curves may be generated by making the expression a function of precipitation temperature and the alumina content (in g/L) within the PBL. A graphical example of the simulation is given below.

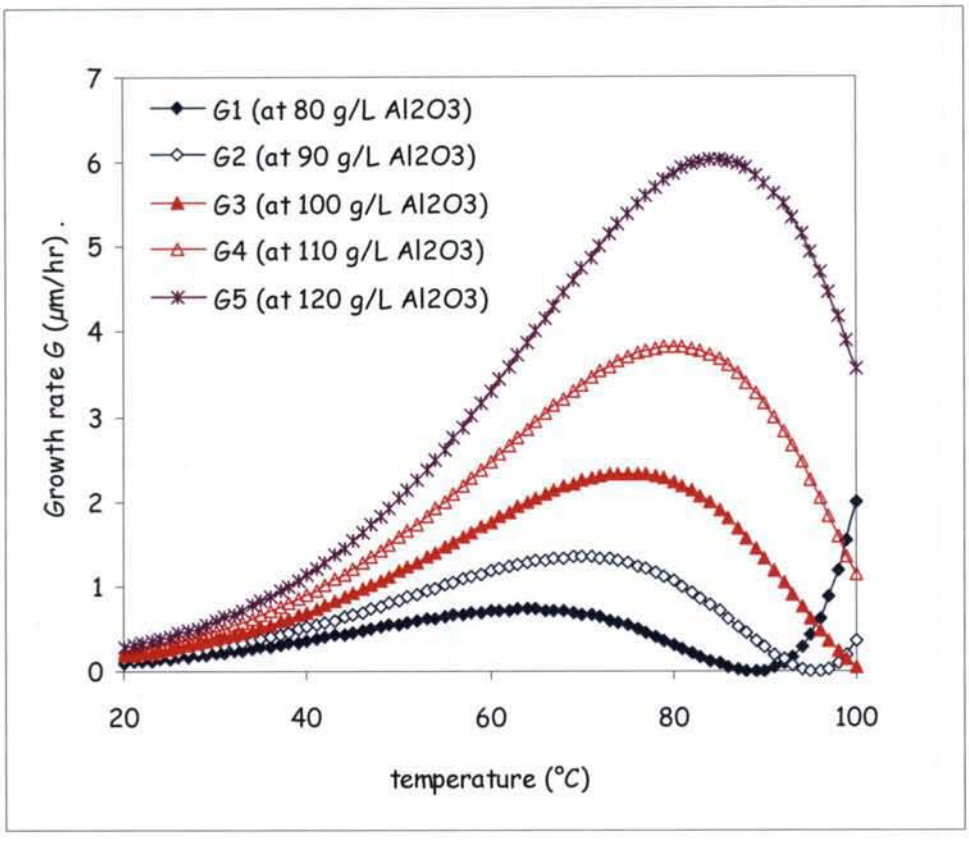

Figure 4: Gibbsite growth curve over a range of precipitation temperatures for various Al_2O_3 content (in g/L) in the Bayer liquor.

The behaviour of the curves in Figure 4 all indicate that there exists a region where the crystal growth rate reaches a maximum. Such plots give a good indication that maximum growth occurs well within the range of 60°C to 90°C (Bayer process conditions). In fact, the model shows an increase in the maximum growth rate temperature as the initially dissolved amount of gibbsite increases. Analytical identification of these maxima can also be calculated by taking the first and second derivatives of Equation 16.

3.5 Effect of caustic concentration

There are several references that discuss the impact of different caustic concentrations on the aluminum speciation in the Bayer liquor. These may serve as information on how the addition of water may affect the resultant gibbsite product quality.

Industrial Bayer liquor with a high caustic content is currently fed into the gibbsite crystalliser at a low alumina supersaturation. A recent study (Li et al., 2003) on the ionic structure of aqueous sodium aluminate suggested evidence of a substantial degree of

hydrogen bonding under high caustic concentrations. These strong bonds promote the clustering of the aluminate monomers $Al(OH)^{4-}$ to form ionic complexes that are poor in mobility. Hence, nucleation does not occur readily in optically clear pregnant Bayer liquors unless precipitation is initiated by seeding.

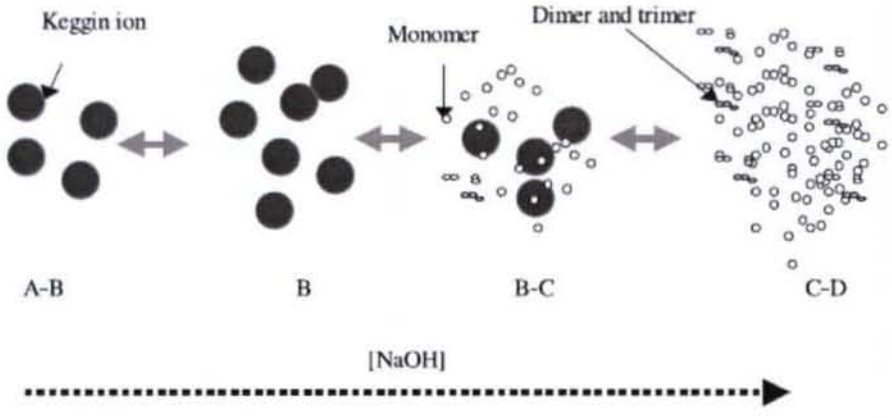

Figure 5: Ionic transformation of alumina complexes across a range of caustic concentrations (Li et al. 2003).

Li et al (2003) also found that the aluminum speciation is only a function of sodium hydroxide concentration, and not dependent on the amount of dissolved alumina hydrate. Furthermore, under a high caustic concentration (NaOH > 4M) the predominant anionic $Al(OH)^{4-}$ monomers engage in spontaneous aggregation (Counter et al., 1999). These were found to occur in a highly structured pattern, eventually forming larger and denser subunits. In contrast, as the dilution of the caustic content in the Bayer liquor increases, the dominant species transforms from the less dense monomers to a denser complex known as Keggin ions. Results by Li et al (2003) showed no evidence that Keggin ions undergo aggregation in optically clear liquors.

3.6 Effect of gibbsite seeding

The purpose of seeding in an industrial PBL is to lower the supersaturation requirement for nucleation and crystal growth by introducing a surface (i.e. a source of pattern) on which further growth can occur. The lowering of the required supersaturation for nucleation and crystal growth spontaneity is due to the lowering of the Gibbs free energy of solid formation (Volmer, 1939).

A study conducted by Li et al. (2006) showed that finer $Al(OH)_3$ seeds produce firmer agglomerates that can better withstand the effect of attrition from agitation. Li also investigated on the effect of initial seed loading on the solid conversion and the total final particle number. The results indicated that while a higher seed loading may result in a higher solid yield, the percentage of particles present in the product classified as fines is also greater due to a higher probability of attrition by particulate collisions.

3.7 An antisolvent for gibbsite precipitation

The use of an antisolvent to re-crystallize gibbsite from PBL has the potential to positively influence the operation of the Bayer Process. This is especially true if the antisolvent can be easily recovered after the re-crystallisation step. Also known as "drowning-out" crystallisation, an antisolvent reduces the solubility of a particular solute in solution, thus promoting crystallisation of that solute. Antisolvents are already used industrially to recover solid products from its solution.

The use of water as an antisolvent to recover gibbsite is based on the overall equilibrium relationship that exists within the Bayer liquor as discussed by Geniesse et al. (2007) and Ilievski (1991):

$$Al(OH)_{3(s)} + NaOH \leftrightarrow NaAl(OH)_4 \leftrightarrow NaAlO_2 + 2H_2O \qquad (17)$$

The addition of water disturbs the above equilibrium, forcing the re-generation of sodium hydroxide (Geniesse et al., 2007) and the gibbsite product. Since water is currently used as a blending agent to adjust the a/c (alumina/caustic) ratio of the pregnant Bayer liquor, no additional reagents and unit operations are required. It is non-toxic and can be removed by evaporation. The current spent liquor recycle stream undergoes evaporation to increase its caustic concentration (Pacific Environmental Services, Inc. 1998).

4. Experimental Methods

4.1 Reactor design

The batch experiments were conducted using a custom-designed stainless steel vessel with PID temperature control. The design specifications used for the vessel followed the procedure stated from Armenante et al. (2006). A simplified diagram is shown below:

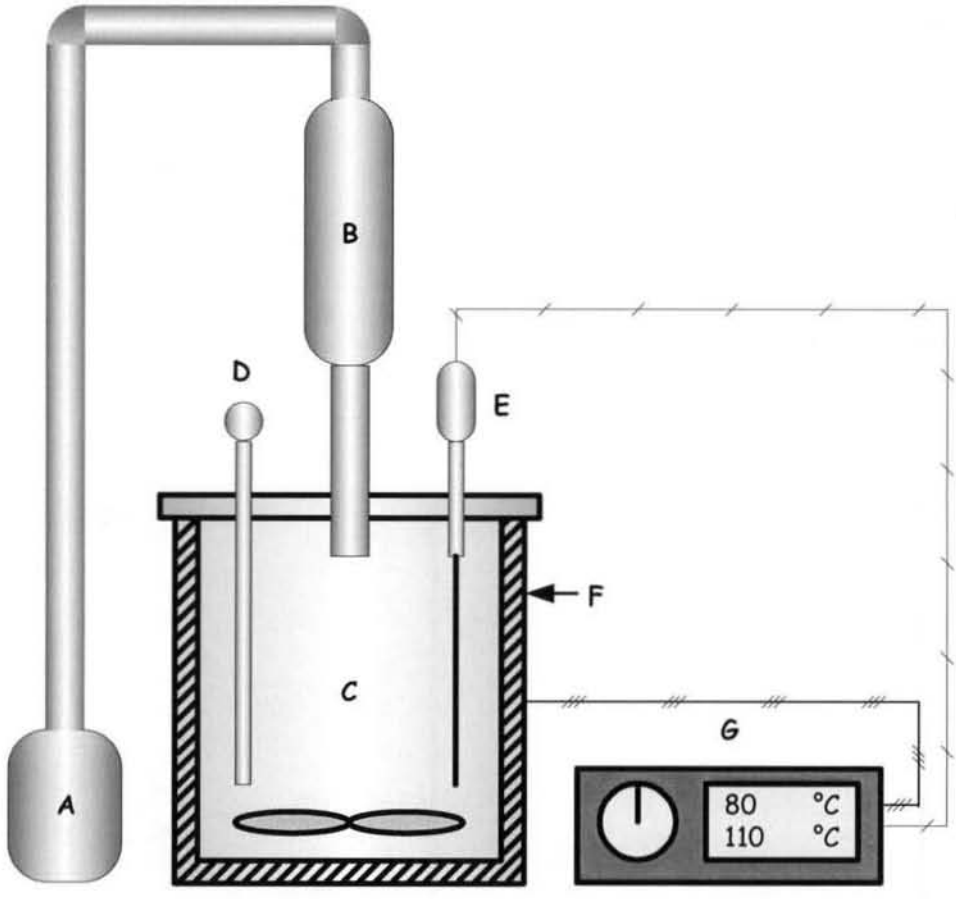

Figure 6: Schematic setup for the batch experiments: A = gas neutralizing flask; B = vapour condenser; C = agitated stainless steel vessel; D = sample/feed port; E = J-type thermocouple; F = heating jacket; G = temperature controller. The condenser chiller is not shown in this diagram.

Isothermal conditions are maintained using a UniTemp PID temperature controller. Electric heating is provided by a stainless steel jacket connected to the controller. The reactor core temperature is read through a J-type thermocouple. This temperature is then automatically adjusted to reach the setpoint temperature of 80°C. At steady state, the precision of the control is 80 ± 0.1°C. An overhead condenser is used to condense any vapour that is formed during precipitation. This is achieved by re-circulating cold water at 5°C on the tube side of the condenser via a Lauda ProLine water bath. Gibbsite product

sampling was taken once every 15 minutes to determine the yield. An experimental period of 4 hours is assigned to every batch.

The basis time of 4 hours was determined from a seeded gibbsite precipitation experiment in the absence of antisolvent addition. This experiment was coded B1 and is assigned the base case run to be used as a reference for all antisolvent precipitation experiments to be conducted in the batch phase.

4.2 Reactor configuration and mixing parameters

In any precipitation system, the physical reactor configuration is significant as it can have an effect on the product characteristics. The placement of baffles, the type of impeller and its clearance, together with the dimension of the reactor shell, all contribute to the efficiency of particle distribution in a seeded precipitation system. A schematic representation of a mechanical agitated vessel with all the important parameters taken from literature is shown on the next page:

Metal sections are all cut and shaped separately. These sections are then welded together to form the reactor body.

4.4 Bayer liquor synthesis

Pregnant synthetic Bayer liquors were synthesized by subjecting hydrated alumina and sodium carbonate to a concentrated solution of sodium hydroxide at an elevated temperature.

The digestion temperature under Bayer refinery conditions usually ranges between 100 ~ 150°C depending on the composition of the bauxite ore. According to Geniesse et al. (2007), the solubility of boehmite (a monohydrated polymorph of alumina) is much lower than its tri-hydrated polymorph (gibbsite). Hence the dissolution of boehmite in caustic soda occurs at a higher temperature than gibbsite.

The laboratory preparation of synthetic Bayer liquor involves the digestion of only tri-hydrated alumina and sodium carbonate in hot caustic soda. The digestion temperature was determined using a trial-and-error method and was found to be about 110°C.

The motivation for the addition of soda ash (Na_2CO_3) during the Bayer liquor synthesis is to produce a carbonated pregnant liquor that resembles the total alkali content (TA) of the gibbsite crystalliser feed. The total caustic content (TC) within the Bayer liquor is a measure of the amount of hydroxide ions present in solution. TA resembles the total concentration of sodium and/or potassium ions present (for the synthetic liquor only one metal species is present). These two parameters are vital since they characterise the precipitation of gibbsite from the Bayer liquor – the dissolution of alumina hydrate increases with an increase in TC, but the precipitation of gibbsite decreases with an increase in TA due to a build-up of carbonate ions from the spent liquor recycle.

The degree of carbonation in the current synthetic liquor will involve the addition of sodium carbonate to achieve a TC/TA feed ratio of 0.8. This conforms to the ratio used in current practice and is kept constant by the addition of lime ($Ca(OH)_2$) to remove carbonate ions as calcite ($CaCO_3$) with caustic re-generation as shown below:

$$Ca(OH)_{2(aq)} + Na_2CO_{3(aq)} \rightarrow CaCO_{3(s)} + NaOH_{(aq)} \qquad (18)$$

The pregnant Bayer liquor synthesized to precipitate gibbsite has the following composition parameters tabulated below:

Table 2: Key parameters describing the nature of pregnant synthetic Bayer liquor.

Parameter(s)	Numerical value	Description
A	126	Alumina concentration in g/L of Al_2O_3
TC	190	Total caustic concentration in g/L of Na_2CO_3
TA	230	Total alkali concentration in g/L Na_2CO_3
A/TC	0.66	Alumina-to-caustic ratio in g/L Al_2O_3 per g/L Na_2CO_3
TC/TA	0.83	Caustic efficiency ratio

From every liquor synthesis, 1 litre of synthetic carbonated caustic aluminate solution was generated prior to the addition of the antisolvent. The synthesis temperature was controlled at 110°C using the UniTemp Advanced PID controller.

~~i.~~ *4.5 Seed preparation*

Seeding used for this study is Alcoa C31 gibbsite seeds. All seeds are pre-treated in spent Bayer liquor for 2 hours prior to every experiment. These seeds are then dried and riffled to obtain a consistent particle size distribution.

4.6 Estimation of synthesis time

Since stainless steel must be used for all equipment constructions, it is not possible to directly observe whether full dissolution of gibbsite has taken place in the hot caustic solution. Alternative methods such as drawing small samples during the liquor synthesis may assist. However, this approach is hazardous as the pressure inside the vessel is slightly elevated due to the high temperature, and occasional build-up of back pressure will cause jets of hot caustics to spontaneously exit the vessel. Hence the estimation of a synthesis period is appropriate to provide a time basis without compromising experimental safety.

The estimation of a synthesis time was based on the method used by Pereira et. al. (2008). The dissolution kinetics were modeled using the analogy of the shrinking nonporous core model around an average gibbsite particle size for a particular load.

4.7 Sample preparation

All samples were drawn isokinetically through a stainless steel sampling port using a precision pipette. The entrance tip of the pipette dispenser has an inner diameter of 1mm (or 1000μm) which is more than 10 times the size of the largest gibbsite particle.

For direct gibbsite solid recovery by filtration for SEM and weight calculations, samples were drawn from the vessel and immediately filtered using Whatman 542 hardened ashless filter paper (pore size = 2.70 μm). The recovered solid was washed thoroughly using de-ionised water to remove the remaining liquor entrained between the particles. These solid samples were then dried at a temperature of less than or equal to 60°C.

For samples undergoing AAS to test for aluminum concentrations, a dilution ratio of 1:500 was applied to all the sample filtrates. A small volume of highly concentrated sodium gluconate (400g/L) was then added to the diluted samples to inhibit further decomposition.

For PSD samples, fixed volumes of slurry were drawn periodically from the reactor and charged into separate 50ml sample flasks. A small injection of highly concentrated sodium gluconate (400g/L) was then added to the samples to inhibit further crystal formation.

For the XRD samples, the gibbsite product was filtered and washed with de-ionised water to remove the entrained Bayer liquor. The wet product was then dried in an oven at a temperature of 60°C. No polymorphic transformations were found when samples were dried at this temperature (Ilievski, 1991). The dried samples were then ground to fine powders using a pestle and mortar before X-ray diffraction analysis was performed.

4.8 Experimental Schedule

Tabulated below are all the experiments conducted in this phase:

Table 3: Experimental schedule of tests conducted as part of the feasibility study.

Test code	Seed loading (g/L)	Antisolvent (ml)	Antisolvent type
B1	50	0	N/A
B2	50	1000	100% H_2O
B3	50	1000	1.5M NaOH in H_2O
B4	50	1000	0.05M NaOH in H_2O
B5	50	1000	100% H_2O
B6	100	1000	100% H_2O

5. Data Analysis

5.1 Product yield

The gibbsite yield can be calculated in two ways namely, by direct sample filtration and weight measurements; and by analyzing the depletion of aluminium ion concentration within the Bayer liquor with time using Atomic Absorption Spectroscopy (AAS). For direct sample weight analysis using filtration, the following equation is used to determine the instantaneous gibbsite yield at the time of sampling:

$$X_{yield} = \frac{(M_{filter} - M_{initial}) - M_{seeds}}{M_{digested}} \times 100 \qquad (19)$$

For the yield calculation from the solution analysis using AAS, the generated aluminum concentration data (normally presented as mg/L of Al) was used.

After a direct comparison between the two methods, it was found that the differences in yield generated from the two methods have a maximum difference of about 20 grams (Figure 8). As expected, gibbsite yield determination by solid recovery was always less than that obtained from AAS.

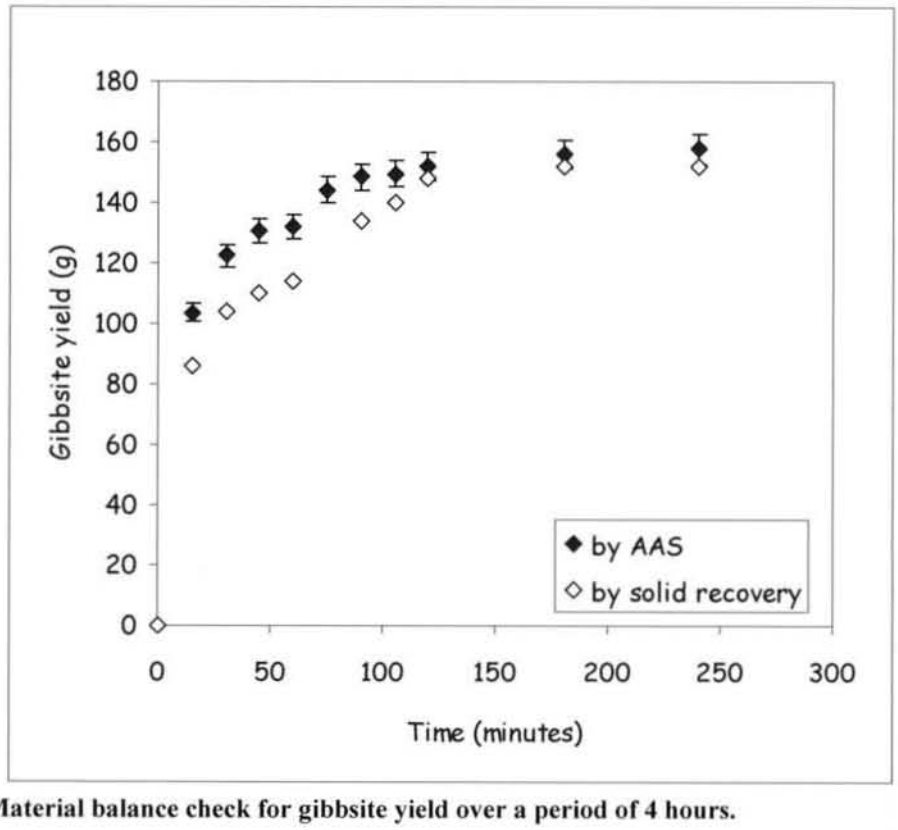

Figure 8: Material balance check for gibbsite yield over a period of 4 hours.

The large discrepancy (± 20%) that arises between these two methods is due to magnification of errors during the scale-up calculation from the sampling volume to the actual reactor volume. For the current study, the stainless steel reactor can accommodate 2 liters of pregnant synthetic Bayer liquor. To achieve this maximum difference, a sample volume of 10ml drawn periodically from this vessel needs only to lose 0.1 grams of product through the steps of filtration, washing, drying and weighing. Thus gibbsite yield determination by AAS is used throughout the course of the batch study.

5.2 Gibbsite impurity check

During the execution of the batch experiments, a simple test is conducted to determine the effect of using glass flasks as liquor transfer media for pregnant Bayer liquor filtration and post-filtration blending to obtain the required A/C ratio.

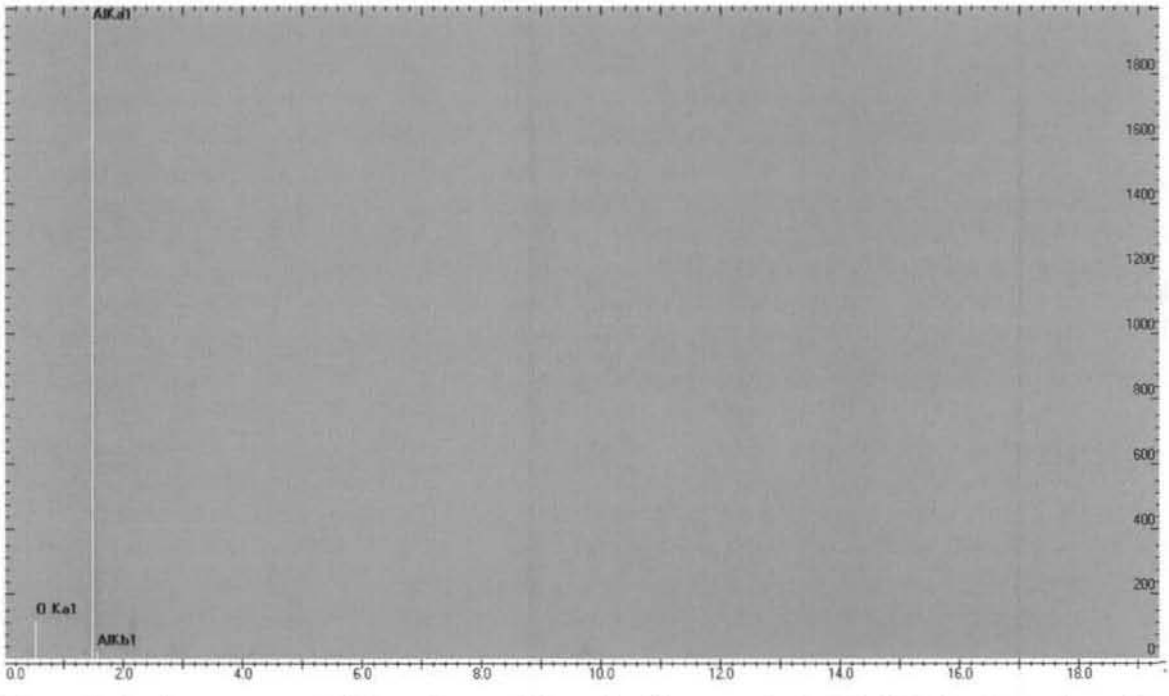

Figure 9: An image generated from Energy-Dispersive X-ray analysis (EDAX) showing only peaks for aluminum and oxygen, but none for silicon.

Energy-Dispersive X-ray analysis (EDAX) was used to detect the presence of impurities in the gibbsite product. This technique involves the preparation of gibbsite samples on a conductive carbon surface. An electron beam is then aimed onto the conductive surface containing the samples causing an emission of X-rays. The energy level of the emitted X-ray is different for various elements present in the sample and is reflected as energy peaks

shown in Figure 9. The absence of the silicon peak is an indication that the use of glassware for the temporary storage of pregnant Bayer liquors does not cause glass etching, a phenomenon often associated with the leaching of silica from borosilicate glassware.

5.3 Particle size distribution

Gibbsite particle sizing and characterisation is conducted via a laser diffraction technique using the Malvern Mastersizer (Model: S Long Bed). This technique compares the extent of laser diffraction due to the presence of particles with a reference incident beam. The amount of deflection as compared from the incident beam is then converted into a volume based percentage.

Although the knowledge to be gained from a volumetric PSD can be significant, knowledge of the corresponding number density PSD is always required to be able to identify the type of crystallisation mechanisms present.

The conversion of the normalized volume-based PSD to a number-based PSD can be carried out in a number of ways. For the current study, the total gibbsite mass calculated from the AAS results are used in conjunction with their corresponding solids to determine the number density of the system.

After determining the gibbsite yield at a particular time, the volumetric yield V_{yield} can be calculated by dividing it with the hydrate density $\rho_{gibbsite}$. From the laser diffraction results, a particle bin size L_1 is chosen together with its corresponding volumetric fraction x_{vol} to arrive at the following expression for total volumetric contribution by particles of a size L_1:

$$V_{L_1} = \frac{M_{sample}}{\rho_{gibbsite}} \cdot x_{vol\_L_1} \tag{20}$$

To obtain the total number of particles per bin size, the total volumetric particle contribution of size L_1 is divided by the volume of a single particle (assuming a sphericity of 1) in L_1:

$$N_{L_1} = \frac{6M_{sample}}{\pi \cdot \rho_{gibbsite} L_1^3} \cdot x_{vol\_L_1} \tag{21}$$

Finally, the total number of particles within the reaction vessel can be determined by integration across all particle sizes that lie in the laser diffraction range:

$$N_{total} = \int_{i=0.01}^{i=1000} \frac{6M_{sample}}{\pi \cdot \rho_{gibbsite} L_i^3} \cdot x_{vol\_L_i} dL \tag{22}$$

5.4 Simultaneous aggregation and growth determination

Because the phenomena of nucleation, growth and aggregation do not occur as separate entities, mathematical estimation of these parameters cannot be conducted independently. Bramley et al. (1996) has developed a method that allows for the simultaneous extraction of precipitation rates directly from experimental PSD data. This method is relevant for this section of the study as it is compatible to parameter estimation in a batch system. The authors arrived at the following set of equations developed using the fundamental concepts of population balance, moment transformation and PSD numerical discretisation:

$$\Phi_0 = \sum_{i=1}^{n} N_{i-1} \sum_{j=1}^{i-2} 2^{j-i+1} f(\bar{L}i-1, \bar{L}j) N_j + \sum_{i=1}^{n} \frac{1}{2} f(\bar{L}i-1, \bar{L}j-1) N^2_{i-1} - \sum_{i=1}^{n} N_i \sum_{j=1}^{i-1} 2^{j-i} f(\bar{L}i, \bar{L}j) N_j - \sum_{i=1}^{n} N_i \sum_{j=1}^{n} f(\bar{L}i, \bar{L}j) N_j$$

$$\Phi_1 = -N_1 \sum_{j=1}^{n} f(\bar{L}_1, \bar{L}_j) N_j$$

$$\Phi_2 = \frac{2}{(1+r)L_1}\left(\left(1 - \frac{r^2}{r^2-1}\right)N_1 - \frac{r}{r^2-1}N_2\right)$$

$$\Phi_3 = \frac{2}{(1+r)L_1}\left(\left(1 - \frac{r^2}{r^2-1}\right)N_1 - \frac{r}{r^2-1}N_2\right)\bar{L}_1^{-3} + \sum_{i=2}^{n} \frac{2}{(1+r)L_i}\left(\frac{r}{r^2-1}N_{i-1} + N_i - \frac{r}{r^2-1}N_{i+1}\right)\bar{L}_i^{-3} \quad (23)$$

The determination of the constants Φ_0, Φ_1, Φ_2 and Φ_3 can all be carried out by directly applying the PSD data obtained from batch sampling (Bramley et al., 1996). In the above equations, *i* is the number of size intervals across the size distribution under investigation. The variable *j* is a running index within the *i* summation that accounts for the possible movements of particles from across size intervals. $\bar{L}i$ is the mean particle size in interval *i* with the corresponding number of particles N_i. The parameter *r* is the geometric discretisation ratio and usually takes on a value of $\sqrt[3q]{2}$ (Li, 2001) where *q* is an integer

that determines the width of the discrete size interval since $L_i+1=rL_i$ (Li 2001) with n being the total number of intervals across the particle size distribution.

Once the above constants are calculated, these can then be used to solve simultaneously for nucleation B_u, crystal growth G and the aggregation kernel β_0 using the expressions listed below (Bramley et al., 1996):

$$\begin{aligned} \dot{m}_0 &= \beta_0 \Phi_0 + B_u \\ \dot{m}_3 &= G\Phi_3 + B_u \bar{L}_1^3 \\ \dot{N}_1 &= G\Phi_2 + \beta_0 \Phi_1 + B_u \end{aligned} \qquad (24)$$

Where: B_u is the source function (m^{-3}/s)

G is crystal growth (m/s)

β_0 is the aggregation kernel (m^3/s)

A detailed derivation of the above expressions can be found in Bramley et al. (1996). A detailed sample calculation illustrating the application of the above method can be found in section 10.2 with the actual kinetic extraction carried out by coding in Mathematica with aid from the DPB toolbox developed by Hounslow (2005).

All particle size distribution curves are shown in section 10.2.

5.5 Agglomeration efficiency and attrition index

Since one of the objectives in this study is to investigate factors affecting the quality of the gibbsite crystals, the product generated from the current investigation must have a certain minimum average particle size to prevent unnecessary loss during transportation. The crystals must also be adequately attrition resistant from mechanical contact. This may be achieved if agglomeration is favoured during the crystallisation process.

According to Wang et. al. (2005), the degree of agglomeration can be quantified using the expression for agglomeration efficiency E_A indicated as follows:

$$E_A = \frac{(i+\eta)\cdot S_2 - i\cdot S_1}{\eta} \times 100\% \quad (25)$$

This expression can be used to determine the agglomeration efficiency of a sample taken at any time during the experiment. S_1 is the fraction of particles in the seeds above 45μm, S_2 is the fraction of particles in the product above 45μm, *i* is the seed-to-liquor ratio and η is the carbonation percentage. Wang and co-workers (2005) defined the degree of carbonation as the amount of carbon dioxide added to the sodium aluminate solution to neutralize the hydroxyl ions.

$$CO_2 + 2OH^- = CO_3^{2-} + H_2O \quad (26)$$

Since the source of carbonate for this study comes from the addition of sodium carbonate (Na_2CO_3), the degree of carbonization is calculated indirectly by performing a mole balance between Equation 32 and the reaction below:

$$Na_2CO_3 + OH^- \rightarrow 2Na^+ + CO_3^{2-} + OH^- \quad (27)$$

Wang and co-workers (2005) quantified the degree of carbonization on a percentage ratio basis but did not show any mathematical expression that defines this expression. Therefore, it is proposed that the following expression is used for the determination of all carbonization percentages for this study in the future:

$$\eta = \frac{M_{co_2}}{M_{PBL}} \times 100 \quad (28)$$

Where: M_{CO2} = mass of dissolved carbon dioxide (g).

M_{PBL} = mass of the PBL before carbonization (g).

The apparent mass of CO_2 can be determined using Equation 32, Equation 33 and a carbonate molecular balance. The mass of the pregnant liquor can be determined by weighing a representative sample drawn using a precision pipette.

For every agglomeration efficiency value quantified, an attrition index is also calculated to better understand the particle processes that take place during the crystallisation of gibbsite. Wang et al. (2005) defined the attrition index as shown in the equation below:

$$I_A = \frac{\gamma_0 - \gamma}{\gamma_0} \times 100 \qquad (29)$$

In Equation 35, γ_0 and γ are the weight percentages of particles with diameters larger than 45μm before and after attrition respectively (Wang et al, 2005).

6. Results and Discussion

6.1.1 Gibbsite purity check

Prior to the commencing of any antisolvent experiments, a trial test is performed in the presence of water as an antisolvent to determine the purity of the gibbsite yield. The XRD analysis generated the following signals:

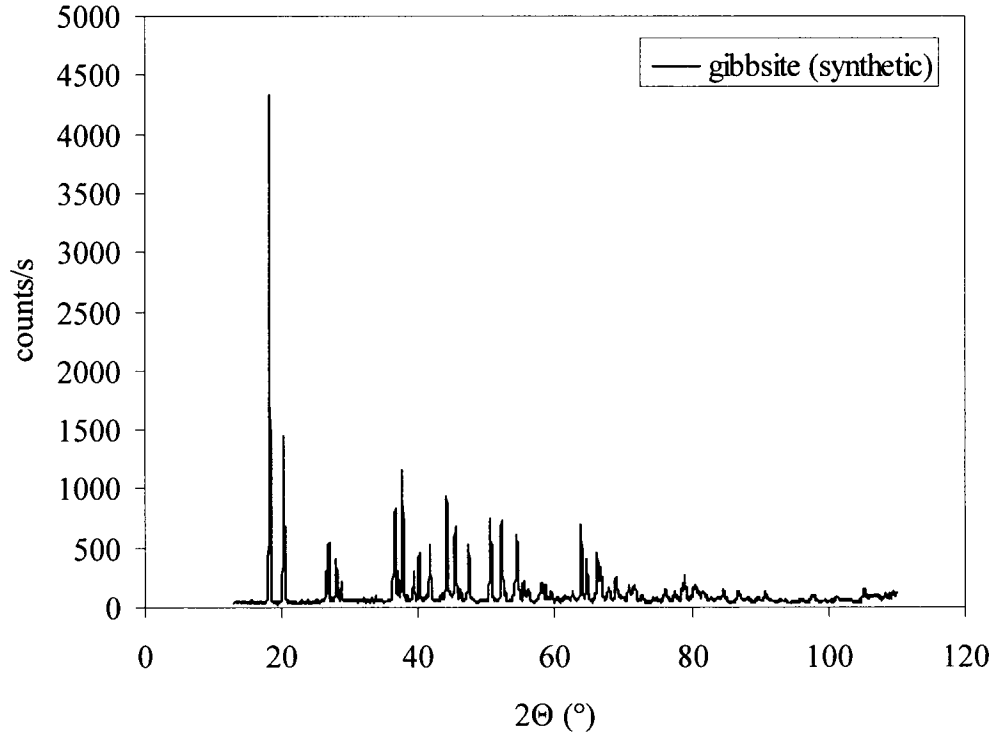

Figure 10: XRD patterns of γ-Al(OH)$_3$ for the final sample taken at the 240th minute during experiment BTCH-5.

From Figure 10, the XRD pattern for a batch sample revealed matching peaks for synthetic gibbsite. The diffraction peaks was found to be 18.2°, 20.3°, 27.9°, 36.5° and 37.3° (Carrier et al. 2006), an indication that there was no undesired polymorphism when gibbsite precipitation experiments were conducted in the presence of water as the antisolvent.

6.2 Effect of antisolvent on product yield

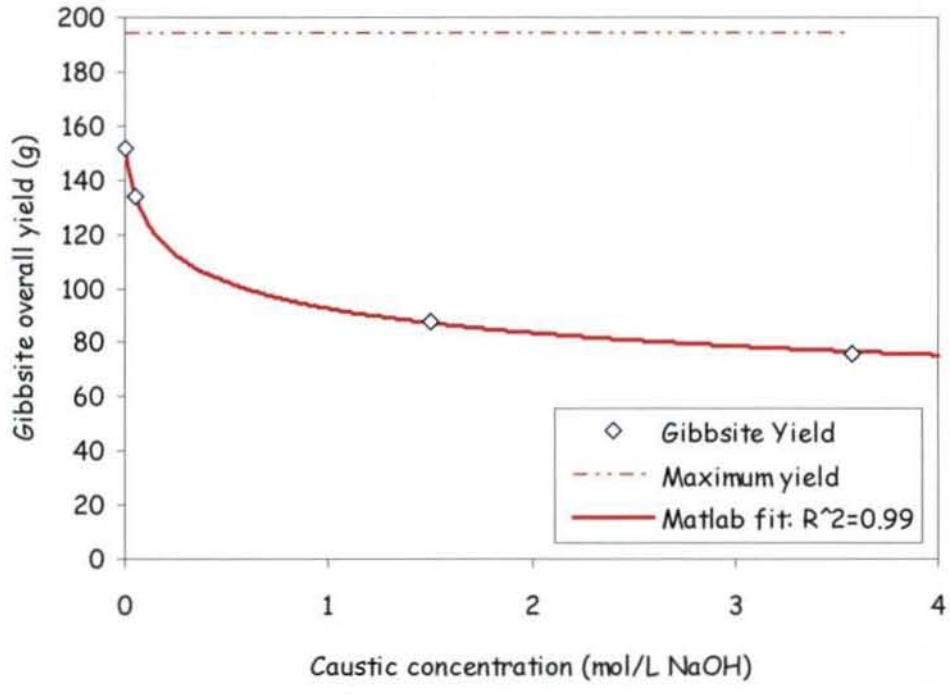

Figure 11: The effect of caustic concentration on the overall gibbsite yield at 80°C.

The effectiveness of an antisolvent relies directly on its purity prior to entering the gibbsite crystalliser. In this study, the strength of the antisolvent represents the quantity of water molecules that are available for reducing the overall caustic concentration of the pregnant Bayer liquor. As predicted, using the model proposed by Rosenberg and Healy (1996), the addition of water as an antisolvent does not change the initial A/C ratio of the pregnant Bayer liquor, since both the alumina and the caustic concentration will decrease at the same rate. However, the model shows that the initial dilution by the antisolvent causes a drop in the equilibrium A/C ratio. This decrease results in an isothermal increase in the corresponding supersaturation for gibbsite precipitation.

From Figure 11, it can be seen that the presence of caustic in water has a significant effect on the final overall yield of the gibbsite product. A non-linear regression performed using MATLAB© shows a power relationship between the overall gibbsite yield and the amount of caustic present in the antisolvent in this operating range. Parameters for the fitted curve are tabulated on the following page.

Table 4: Constants from a curve fitting performed in MATLAB©.

Equation type fitted:	$f(x) = a(x+b)^n$
Constants:	a = 93.126; b = 0.039546; n = -0.1515

The original curve fitting together with the MATLAB© codes is available in section 10.1.

6.3 Effect of seed loading on product yield

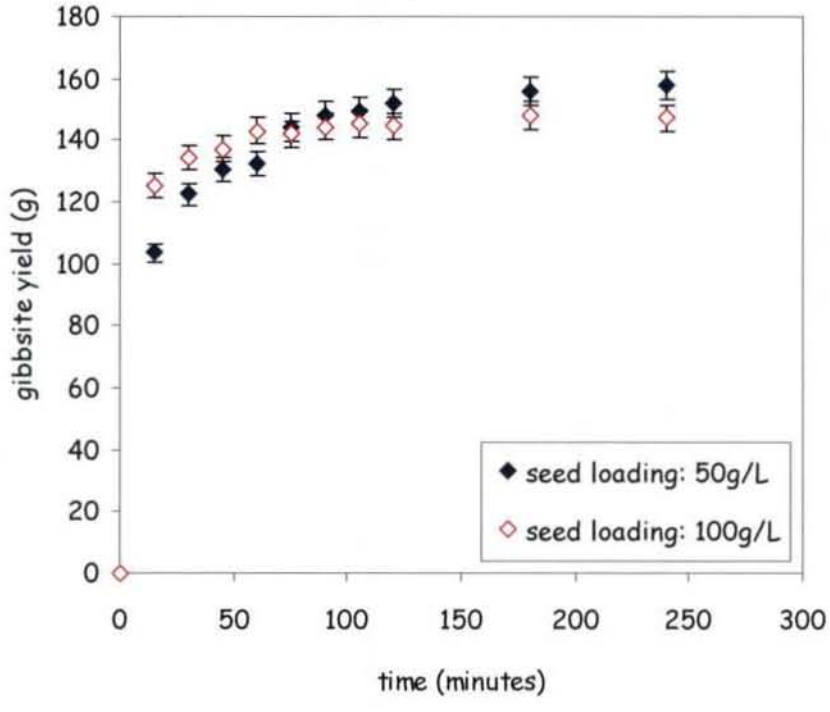

Figure 12: Resultant gibbsite yield characteristics from different seed loadings per litre of synthetic liquor at 80°C in the presence of an antisolvent.

Graphical results for the seed loading experiments are shown in Figure 12 and Figure 13. The curve generated at the higher seed loading indicates a slightly higher product yield between t = 0 and 90 minutes. However at the later stages of precipitation, it was found that, by conducting the experiment at a lower seed loading, a slightly higher overall product yield is achieved.

Similar phenomena on intersecting product curves were documented in the past gibbsite literature involving batch precipitation under various seed loadings (Li et al., 2000). In the paper by Li et al. (2000), two curves showing the amount of new crystals formed with

time for two different seed loadings were presented. The graphs generated from the experiments also exhibit an intersection for the net number of crystals formed during two experiments under different seed loadings. The authors suggested that the phenomenon is due to a much faster desupersaturation rate as a result of a higher seed surface area. This statement is further confirmed by Ilievski (2006) where a higher solid loading leads to a much flatter desupersaturation curve.

Since the main particle processes in any precipitation system are nucleation, crystal growth and aggregation, it is plausible (for the purpose of this feasibility study) to suggest that the phenomena stated by Li et al (2000) are the main contributing factors influencing the shape of gibbsite yield curve. This statement is based upon the finding that gibbsite crystal growth is not dominant (7×10^{-9} $m.s^{-1}$) and aggregation is mass conserving.

A quantitative comparison between the present values for $ß_0$ and G and those obtained from studies conducted by Li (2000) revealed that the both parameters lie within their expected orders of magnitude: 10^{-7} $m^3.s^{-1}$ for aggregation and 10^{-9} $m.s^{-1}$ for growth. However, comparisons for the average gibbsite particle size in the yield between the work by Li and the present work indicated an expected drop in average size. The size range obtained by Li lies between 20μm and 80μm whereas the size range obtained from the current feasibility study lies between 0.1μm and 0.7μm at the lower seed loading of 50 grams gibbsite where lower inter-particulate attrition is experienced (Li et al. 2006).

The above findings suggest nucleation to be the main phenomenon responsible for the overall shape of the yield curves. This is especially true since the presence of an antisolvent isothermally increases the supersaturation driving force of aluminum within the Bayer liquor by decreasing its equilibrium solubility. This increase in supersaturation favours the mechanism of nucleation (Myerson 2002). The combination of nucleation and increased inter-particulate collision at the higher seed loading (Li et al. 2006) results in the initial breeding.

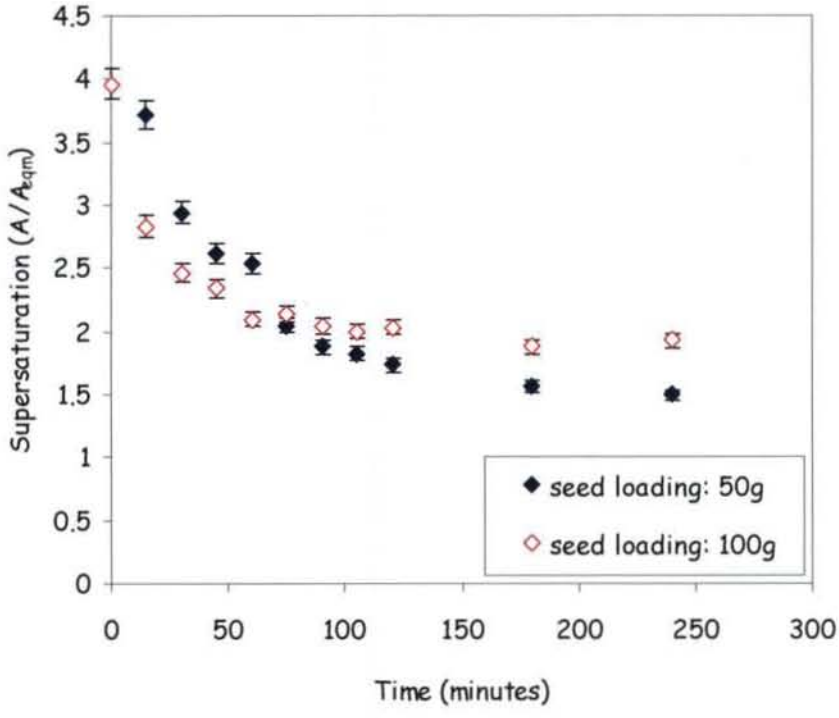

Figure 13: Desupersaturation characteristics of pregnant Bayer liquor from different seed loadings at 80°C in the presence of an antisolvent.

Figure 14 shows a set of gibbsite SEMs taken from the experiment with the lower seed loading. It can be seen that both aggregation and structured crystal shape development are evident. The resultant geometry for gibbsite in the SEM is hexagonal which conforms to the morphology discussed from previous studies (Blanks 1999).The gibbsite morphology at t = 240 minutes shows development under low shear.

(1) At t = 0 minutes

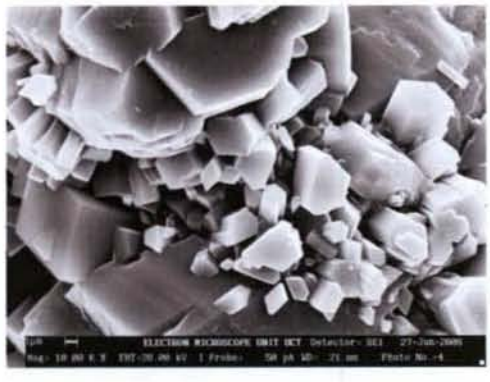

(2) At t = 240 minutes

Figure 14: SEM monitoring of gibbsite morphology development at a lower seed loading (50 grams).

By comparing the gibbsite morphology development under identical initial supersaturations with different seed loadings, it can be seen that the crystal structure shown in Figure 15 shows contrasting features in terms of aggregation and inter-particulate collision. Since previous studies suggested that conducting precipitation experiments at a higher seed loading results in a rise in inter-particulate attrition, an intermediate sample was taken for SEM to qualitatively determine the extent of attrition under such conditions.

(1) At t = 0 minutes.

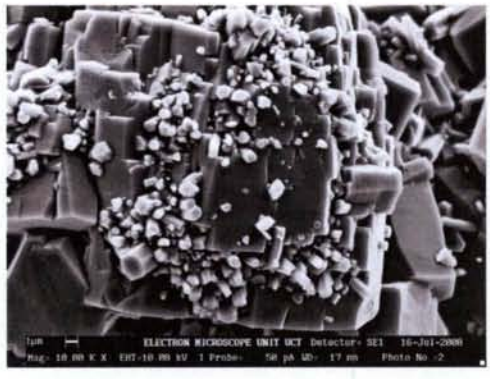

(2) At t = 120 minutes.

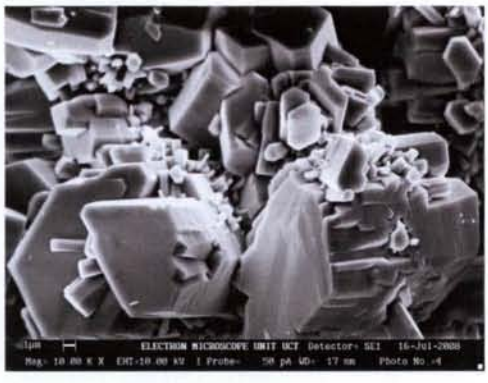

(3) At t = 240 minutes.

Figure 15: SEM monitoring of gibbsite morphology development at a higher seed loading (100 grams).

From Figure 15, by comparing the morphology from t = 0 minutes to t = 240 minutes, it is evident that aggregation and structured crystal growth are present, however the "packed" nature of the crystals suggests that aggregation is dominant over growth.

By comparing the development of the crystallites on the surface of the crystals between Figure 14 and Figure 15, the effect of inter-particulate attrition is clear. It is also possible

that initial breeding occurred. Physical evidence gathered from the SEM shows lack of crystallite development between t = 120 minutes and t = 240 minutes in the presence of a higher seed loading. In fact, hardly any of the crystallites detected at t = 120 minutes remained when the final sample was analysed.

Furthermore, the last gibbsite sample in Figure 15 indicated stress and fatigue marks that were not observed in Figure 14. These marks, together with the lack of crystallites in the parent surface, suggest inter-particulate attrition and possibly secondary nucleation as a result.

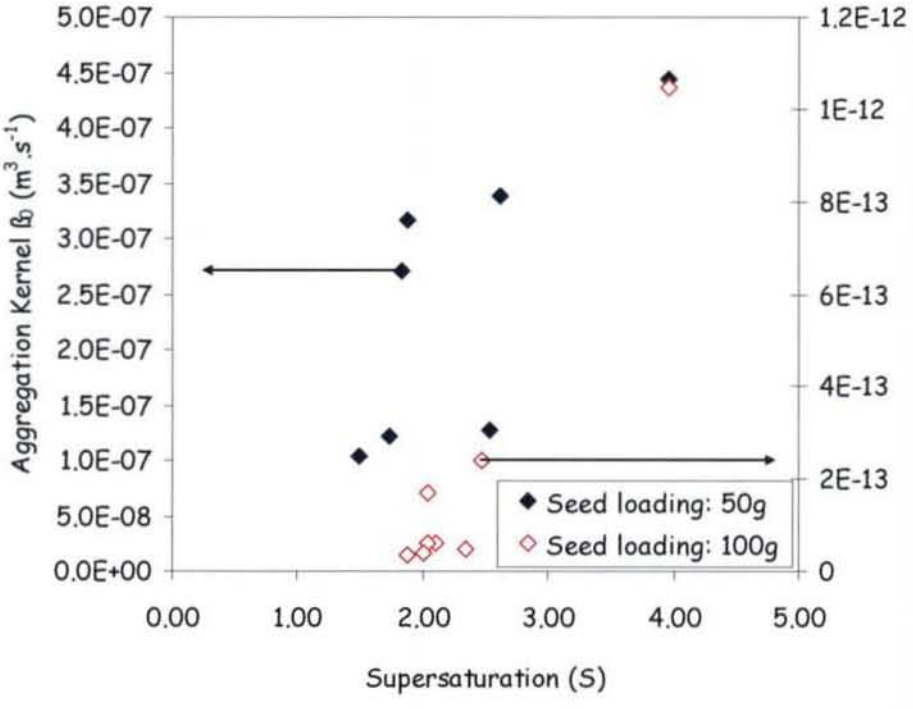

Figure 16: Aggregation kernel $ß_0$ estimation as a function of liquor supersaturation at a temperature of 80°C and 435rpm for different seed loadings.

The relationship between the aggregation kernels and their corresponding supersaturations shown in Figure 16 indicates a direct correlation in which increased supersaturation favours the aggregation mechanism. This behaviour may be due to the gibbsite-liquor system approaching the isoelectric point (pH = 9) after the addition of water. The obtained data trend is very similar to an experiment conducted by Ilievski and Livk (2006) indicating this direct relationship. As expected, the presence of an

antisolvent causes supersaturations at the minimum aggregation kernel for both experiments to be higher than that obtained by Ilievski & Livk (2006). This could also be due to the higher collision rates associated with antisolvent addition since the liquor viscosity decreased.

Furthermore, it was also found that the $ß_0$ obtained at the higher seed loading is much smaller, indicating increased aggregate collision frequency causing a rise in attrition rates (Ilievski & Livk 2006; Li et al. 2006).

6.4 Effect of seed loading on fines formation

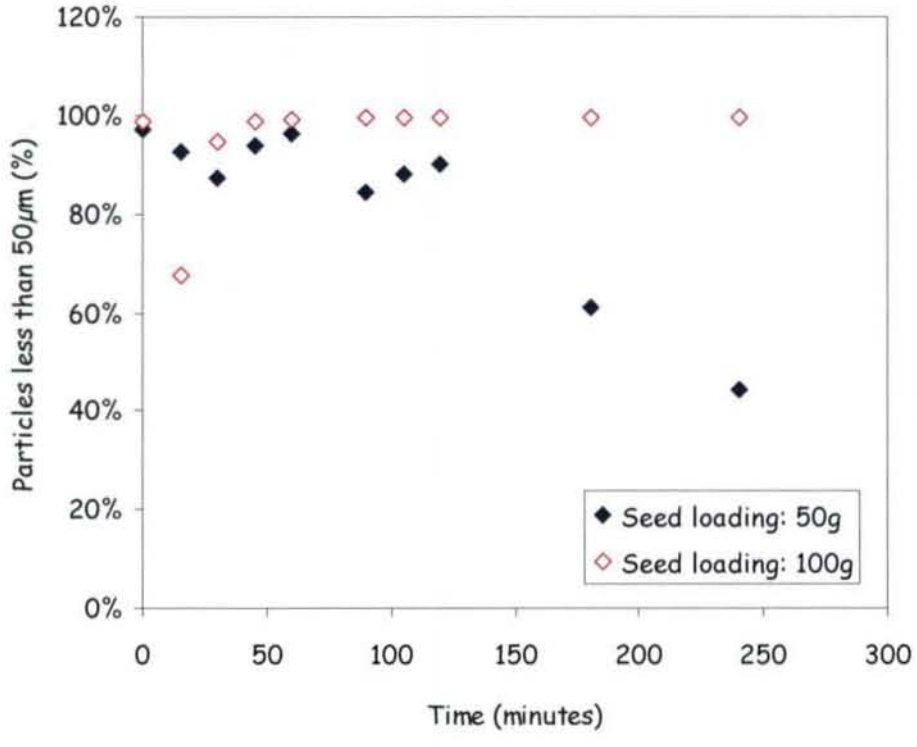

Figure 17: Changes in the percentage of particles less than 50μm.

The analysis for fines formation under different seed loadings can be conducted by comparing the curves in Figure 17. A reference gibbsite particle size of 50μm is chosen. This size lies within the range of the expected particles sizes for the gibbsite precipitate found from previous studies (Ilievski 1991; Li 2001).

It can be seen that, even under the presence of an antisolvent, the system with the higher initial seed loading yields finer particles. This is probably due to the increased inter-particulate collisions at the higher seed loading (Li et al. 2006).

It was also found that aggregation was dominant at the early stages (at time < 50 minutes) of gibbsite precipitation when a higher seed loading was used. According to Li et al., (2006), this is due to aggregation being a phenomenon that occurs readily to reduce the surface energy in a particulate system. Furthermore, the finer gibbsite particle possesses a higher activity (Li et al. 2006) making the mechanism of aggregation more prominent. However due to the higher seed loading, the effect of inter-particulate collision became dominant at later stages of precipitation, causing a drop in mean gibbsite particle size.

As the batch experiments were conducted using an agitated vessel, higher seed loadings did not inhibit the fines formation of the gibbsite precipitate. The above phenomena were consolidated from previously conducted experiments from literature (Ilievski & Livk, 2006; Li et al., 2006). However, if the same principle was applied to the operation of a fluidised bed reactor, an improvement in gibbsite fines inhibition is expected due to the low particulate shear associated with its hydrodynamics (Lewis, 2006).

Despite the larger mean particle size arising from the application of a lower seed loading, the increase in alumina supersaturation from the antisolvent addition caused an overall drop in mean particle size when compared to batch experiments conducted in the absence of antisolvents under similar conditions (Li, 2001) where the mean particle size ranges from 10μm to 100μm.

7. Conclusions

The batch feasibility study of antisolvent gibbsite precipitation was conducted isothermally at a temperature of 80°C.

The results indicated that water is a feasible antisolvent to increase the overall yield of the gibbsite precipitate. The overall yield exhibits a power law dependency on its Bayer caustic concentration.

An increase in seed loading under constant temperature and initial liquor supersaturation resulted in an overall decrease in product particle size. This phenomenon is mainly due to a rise in overall collision frequency between the gibbsite particles which resulted in solid rupture. Quantitative evidence of this mechanism is shown using the discretised population balance method by Bramley et al. (1996) with the aid of a computational technique developed by Hounslow (2005) using Mathematica software. Results generated using this method show decreasing aggregation with liquor desupersaturation and increased seed loading.

The overall particle behaviours from the current investigation are validated by results obtained from previous gibbsite studies under very similar conditions. Although the gibbsite yield can be increased drastically in the presence of an antisolvent, the average particle size generated from this study is still too small to be commercially feasible due to the increase in initial supersaturation. Further particle size optimisation can be conducted inside a fluidised bed reactor where particles generally experience lower shear than inside a conventional agitated vessel. The mechanism of aggregation is expected to be dominant is this reactor configuration.

8. Recommendations

8.1 A fluidised bed approach

Fluidised bed reactors (FBR) are commonly used to remove metals impurities from industrial waste water streams by seeded precipitation. These reactors offer good metal removal efficiency and solid characteristics if the global supersaturation of the reaction system is low. This is vital since systems with extremely low solubilities generate a high global supersaturation, resulting in a poor control with regards to fines formation due to spontaneous nucleation (Lewis, 2006). The low shear experienced by the fluidised particle in a FBR ensures that fines formation from agglomerate attrition is minimized. In addition to the low shear characteristics, the hydrodynamics in a FBR are such that there is a better distribution of the local supersaturation thus minimising dead spaces within the reaction volume.

Thus, in the context of antisolvent gibbsite crystallisation, the use of a FBR for the control of local supersaturation using multiple side feeds in a fluidised bed reactor (Lewis, 2006), together with criteria presented above, indicated good potential for using the FBR for industrial gibbsite production.

The isothermal introduction of water increases the supersaturation of alumina in the Bayer liquor by decreasing its caustic concentration. The application of side feeds offers better distribution of local supersaturation which, in turn, minimises fines formation. Since the crystallisation of gibbsite is a slow process, a long residence time is required to achieve a high conversion. This requires a low feed velocity (or a larger reactor volume) in fluidised operations. The low feed rate also minimizes fines formation via inter-particulate attrition while promoting intimate fluidised mixing.

While the addition of water may improve the overall conversion of gibbsite, previous investigations by Li et al. (2003) suggests that the dilution of the pregnant liquor results in a change in aluminum speciation under isothermal conditions. Consequently, whilst the attrition rate and local supersaturation is controlled by different reactor configuration, the change in aluminum speciation across varying caustic concentrations due to dilution may affect the quality of the gibbsite product.

9. References

Addai-Mensah, J., Dawe, J., Hayes, R., Prestidge, C. & Ralston, J. 1998, "The Unusual Colloid Stability of Gibbsite at High pH", vol. Journal of Colloid and Interface Science, no. 203, pp. 115-121.

Armenante, P.M., Atiemo-Obeng, V. & Penney, W.R. 2006, "Multiphase Mixing and Solid-Liquid Mixing in Agitated Reactors" in Encyclopedia of Chemical Processing Taylor & Francis, New York, pp. 1767-1777.

Blanks, K.A. 1999, Laser Precipitation of Sodium Aluminate Solutions, 204/157.41 edn, C01F 7/00, United States of America.

Bramley, A.S., Hounslow, M.J. & Ryall, R.L. 1996, "Aggregation during Precipitation from Solution: A Method for Extracting Rates from Experimental Data", Journal of Colloid and Interface Science, vol. 183, pp. 155-165.

Carrier, X., Marceau, E., Lambert, J. & Che, M. 2006, "Transformation of γ-alumina in aqueous suspensions: 1. Alumina chemical weathering studied as a function of pH", Journal of Colloid and Interface Science, vol. 308, pp. 429-437.

Chen, Y., Feng, Q., Liu, K., Chen, Y. & Zhang, G. 2006, "Study on the structure of Bayer liquor with spectroscopy and MD simulation", Chemical Physics Letters, vol. 422, pp. 406-411.

Counter, J.A., Addai-Mensah, J. & Ralston, J. 1999, "The formation of Al(OH)3 crystals from supersaturated sodium aluminate solutions revealed by cryovitrication-transmission electron microscopy", Colloids and Surfaces A: Physicochemical and Engineering Aspects, vol. 154, pp. 389-398.

Davidson, J.F., Clift, R. & Harrison, D. 1985, Fluidization, 2nd edition edn, Academic Press, London.

Geniesse, D., Nelson, E. & Stegen, G. 2007, Modified Bayer Process for Alumina Removal from Hanford Waste, Areva NC, Inc.

Giulietti, M., Seckler, M.M., Derenzo, S., Ré, M.I. & Cekinski, E. 2001, "Industrial Crystallization and Precipitation from Solutions – State of the Technique", Braz. J. Chem. Eng., vol. 18, no. 4, pp. 1-24.

Harrison, D., Keir, R.I., Prestidge, C.A. & Thomas, J.C. 1999, "A dynamic light scattering investigation of nucleation and growth in supersaturated alkaline sodium aluminate solutions (synthetic Bayer liquors)", Colloid and Surfaces A: Physicochemical and Engineering Aspects, vol. 154, pp. 343-352.

Hounslow, M.J. 1990, "A Discretized Population Balance for Continuous Systems at Steady State", AIChE Journal, vol. 36, no. 1, pp. 106-116.

Hounslow, M.J., Lewis, A.E., Sanders, S.J. & Bondy, R. 2005, "Generic Crystallizer Model: I. A Model Framework for a Well-Mixed Compartment", Particle Technology and Fluidization, vol. 51, no. 11, pp. 2942-2955.

Ikkatai, T. & Okada, N. 1963, "Viscosity, Specific Gravity and Equilibrium Concentration of Sodium Aluminate Solutions", Extractive Metallurgy of Aluminium, vol. 1, pp. 159-173.

Ilievski, D. 1991, Modelling Al(OH)3 Agglomeration During Batch and Continuous Precipitation in Supersaturated Caustic Aluminate Solutions, University of Queensland.

Ilievski, D. & Livk, I. 2006, "An agglomeration efficiency model for gibbsite precipitation in a turbulently stirred vessel", Chemical Engineering Science, vol. 61, pp. 2010-2022.

Karbanee, N. 2007, An Investigation into Precipitation of Cobalt Sulphide and Nickel Sulphide from the Aqueous Stream after the Nickel Reduction Process, University of Cape Town.

Lewis, A.E. 2006, "Fines Formation (and Prevention) in Seeded Precipitation Processes", KONA, vol. 24, pp. 119-125.

Li, H., Addai-Mensah, J., Thomas, J.C. & Gerson, A.R. 2003, "A study of colloidal Al(III)-containing species in fresh/caustic aluminate solutions", Colloids and Surfaces A: Physicochem. Eng. Aspects, vol. 223, pp. 83-94.

Li, J., Prestidge, C.A. & Addai-Mensah, J. 2000a, "Viscosity, Density, and Refractive Index of Aqueous Sodium and Potassium Aluminate Solutions", Journal of Chemical Engineering Data, vol. 45, pp. 665-671.

Li, J., Prestidge, C. & Addai-Mensah, J. 2000b, "Secondary nucleation of gibbsite crystals from synthetic Bayer liquors: effect of alkali metal ions", Journal of Crystal Growth, vol. 219, pp. 451-464.

Li, T.S. 2001, Modelling and Kinetics Estimation in Gibbsite Precipitation from Caustic Aluminate Solutions, Curtin Unversity of Technology.

Li, T.S., Livk, I. & Ilievski, D. 2001, "The influence of crystalliser configuration on the accuracy and precision of gibbsite crystallisation kinetics estimates", Chemical Engineering Science, vol. 56, pp. 2511-2519.

Li, X., Feng, G., Zhou, Q., Peng, Z. & Liu, G. 2006, "Phenomena in late period of seeded precipitation of sodium aluminate solution", Transactions of Nonferrous Metals Society of China, vol. 16, pp. 947-950.

Löffelmann, M. & Mersmann, A. 2002, "How to measure supersaturation?", Chemical Engineering Science, vol. 57, pp. 4301-4310.

Ma, S., Zheng, S. & Xu, H.Z., Y. 2007, "Spectra of sodium aluminate solutions", *Transaction of nonferrous Metals Society of China,* vol. 17, pp. 853-857.

McColl, P. & Welton, R. 2001, Production of Alumina, 423/122, 423/121 ,423/127 edn, USA.

Misra, C. 1970, The precipitation of Bayer aluminium trihydroxide, University of Queensland.

Mostafa Nowee, S., Abbas, A. & Romagnoli, J.A. 2008, "Antisolvent crystallization: Model identification,experimental validation and dynamic simulation", Chemical Engineering Science, vol. 63, pp. 5457-5467.

Mydlarz, J. & Jones, A.G. 1989, "Growth and dissolution kinetics of potassium-sulfate crystals in aqueous 2-propanol solutions", Chemical Engineering Science, vol. 44, no. 6, pp. 1391-1402.

Myerson, A. 2002, Handbook of Industrial Crystallization, 2nd edn, Butterworth Heinemann, Oxford.

Pacific Environmental Services, I. 1998, Background Report AP42 Section 12.1 Primary Aluminum, Research Triangle Park, NC.

Pina, C.M., Fernandez-Diaz, L., Prieto, M. & Veintemillas-Verdaguer, S. 2001, "Metastability in drowning-out crystallisation: precipitation of highly soluble sulphates", Journal of Crystal Growth, vol. 222, pp. 317-327.

Prestidge, C.A., Ametov, I. & Addai-Mensah, J. 1999, "Rheological investigations of gibbsite particles in synthetic Bayer liquors", Colloids and Surfaces A: Physicochemical and Engineering Aspects, vol. 157, pp. 137-145.

Rosenberg, S.P. & Healy, S.J. 1996, "A thermodynamic model for gibbsite solubility in Bayer liquor", 4th International Alumina Quality WorkshopDarwin, Australia, pp. 301.

Rossiter, D.S., Fawell, P.D., Illievski, D. & Parkinson, G.M. 1998, "Investigation of the unseeded nucleation of gibbsite, Al(OH)3, from synthetic bayer liquors", Journal of Crystal Growth, vol. 191, pp. 525-536.

Sakamoto, K. 1963, "Extractive Metallurgy of Aluminium", Interscience Publishers, vol. 1, pp. 175-189.

Vernon, C. 2008, TC/TA Ratio in the Bayer Process.

Volmer, M. 1939, Kinetics der Phasenbildung, Steinkoff, Dresden.

Wang, Z., Bi, S., Yang, Y. & Yuan, Z. 2005, "Evolution of particle size and strength of hydragillite from carbonization in seeded sodium aluminate liquors", Journal of Crystal Growth, vol. 274, pp. 218-225.

White, E.T. & Bateman, S.H. 1988, "Effect of Caustic Concentration on the Growth Rate of Al(OH)3 Particles", Light Metals, vol. 88, pp. 257-262.

Wolfram Software 2000, Mathematica.

Yeo, S. & Lee, J.C. 2004, "Crystallization of sulfamethizole using the supercritical and liquid antisolvent processes", Journal of Supercritical Fluids, vol. 30, pp. 315-323.

Zámbó, J. 1986, "The Structure of Sodium Aluminate Liquors: Molecular Model of the Mechanisms of their Decomposition", Light Metals, , pp. 199-215.

Zhang, Y., Zheng, S., Du, H., Xu, H., Wang, S. & Zhang, Y. 2009, "Improved precipitation of gibbsite from sodium aluminate solution by adding methanol", Hydrometallurgy, vol. 98, pp. 38-44.

Zijlema, T.G., Geertman, R.M., Witkamp, G., van Rosmalen, G.M. & de Graauw, J. 2000, "Antisolvent Crystallization as an Alternative to Evaporative Crystallization for the Production of Sodium Chloride", Ind. Eng. Chem. Res., vol. 39, pp. 1330-1337.

10. Appendices

10.1 Conversion feasibility data

Gibbsite conversion plot

A/C: 0.67

C: 194 g/L Na_2CO_3

S (ratio): 1.821

Al(OH)3 content: 194 g/L

Seed load: 50g/L $Al(OH)_3$

Exp code: B1

Time (min)	Filter (g)	Filter + ppt (g)	ppt (g/L)	conversion by wt (%)
0	0.45	0.95	0.00	0.00%
15	0.45	1.10	15.00	12.38%
30	0.45	1.36	41.00	33.83%
45	0.45	1.43	48.00	39.60%
60	0.45	1.40	45.00	37.13%
90	0.44	1.58	64.00	52.81%
105	0.44	1.56	62.00	51.16%
120	0.44	1.55	61.00	50.33%
180	0.45	1.68	73.00	60.23%
240	0.44	1.70	76.00	62.71%
1500	0.44	1.96	102.00	84.16%

Gibbsite conversion plot

A/C: 0.67

C: 194 g/L Na_2CO_3

S (ratio): 3.989

Al(OH)3 content: 194 g/L

Seed load: 50g/L $Al(OH)_3$

Exp code: B2

Time (min)	Filter (g)	Filter + ppt (g)	ppt (g/2L)	conversion by wt (%)
0	0.45	0.70	0.00	0.00%
15	0.45	1.13	86.00	54.54%
30	0.45	1.22	104.00	65.96%
45	0.45	1.25	110.00	69.77%
60	0.46	1.28	114.00	72.30%
90	0.45	1.37	134.00	84.99%
105	0.45	1.40	140.00	88.79%
120	0.45	1.44	148.00	93.87%
180	0.45	1.46	152.00	96.40%
240	0.45	1.46	152.00	96.40%

Gibbsite conversion plot

A/C: 0.67

C: 194 g/L Na_2CO_3

S (ratio): 3.952 (NaOH = 1.5M)

Al(OH)3 content: 194 g/L

Seed load: 50g/L $Al(OH)_3$

Exp code: B3

Time (min)	Filter (g)	Filter + ppt (g)	ppt (g/2L)	conversion by wt (%)
0	0.45	0.70	0.00	0.00%
15	0.45	0.90	40.00	28.58%
30	0.44	0.91	44.00	31.43%
45	0.45	0.92	44.00	31.43%
60	0.44	0.93	48.00	34.29%
90	0.45	0.95	50.00	35.72%
105	0.45	0.97	54.00	38.58%
120	0.45	0.99	58.00	41.43%
180	0.44	1.06	74.00	52.86%
240	0.45	1.14	88.00	62.87%

Gibbsite conversion plot

A/C: 0.67

C: 194 g/L Na_2CO_3

S (ratio): 3.988 (NaOH = 0.05M)

Al(OH)3 content: 194 g/L

Seed load: 50g/L $Al(OH)_3$

Exp code: B4

Time (min)	Filter (g)	Filter + ppt (g)	ppt (g/2L)	conversion by wt (%)
0	0.45	0.70	0.00	0.00%
15	0.45	0.76	12.00	8.57%
30	0.45	0.83	26.00	18.57%
45	0.45	0.88	36.00	25.72%
60	0.45	0.93	46.00	32.86%
75	0.44	0.95	52.00	37.15%
90	0.44	1.06	74.00	52.86%
105	0.44	1.18	98.00	70.01%
120	0.45	1.30	120.00	85.73%
180	0.46	1.38	134.00	95.73%
240	0.44	1.36	134.00	95.73%

EXP CODE:	B1	B2	B3	
Time (min)	ppt (g)	ppt (g)	ppt (g)	Abs. max (g)
0	0	0	0	194
15	15	86	40	194
30	41	104	44	194
45	48	110	44	194
60	45	114	48	194
90	64	134	50	194
105	62	140	54	194
120	61	148	58	194
180	73	152	74	194
240	76	152	88	194

EXP CODE:	B4
Time (min)	ppt (g)
0	0
15	12
30	26
45	36
60	46
90	74
105	98
120	120
180	134
240	134

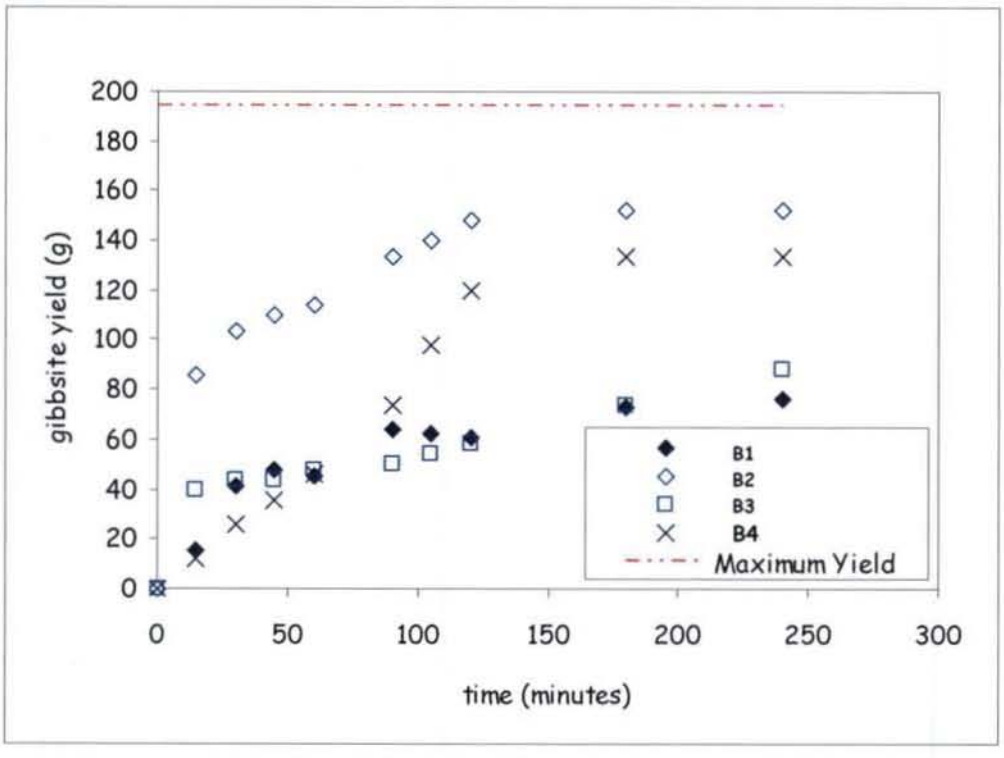

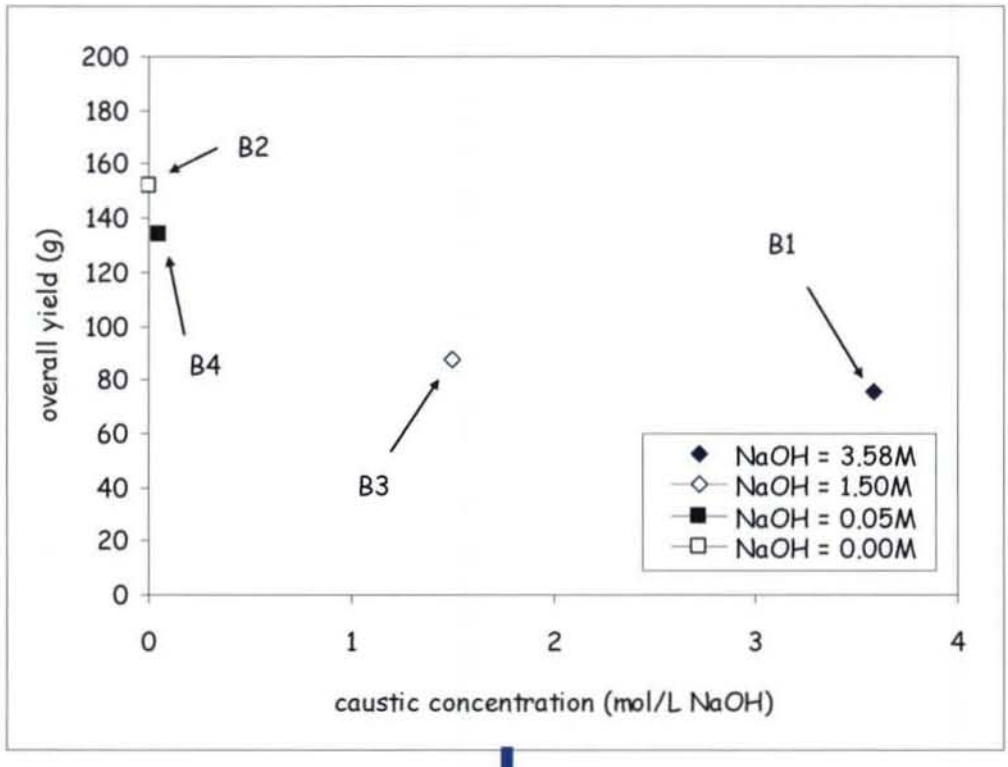
200
180
160
140
120
100
80
60
40
20
0
overall yield (g)
B2
B1
B4
B3
NaOH = 3.58M
NaOH = 1.50M
NaOH = 0.05M
NaOH = 0.00M
0
1
2
3
4
caustic concentration (mol/L NaOH)

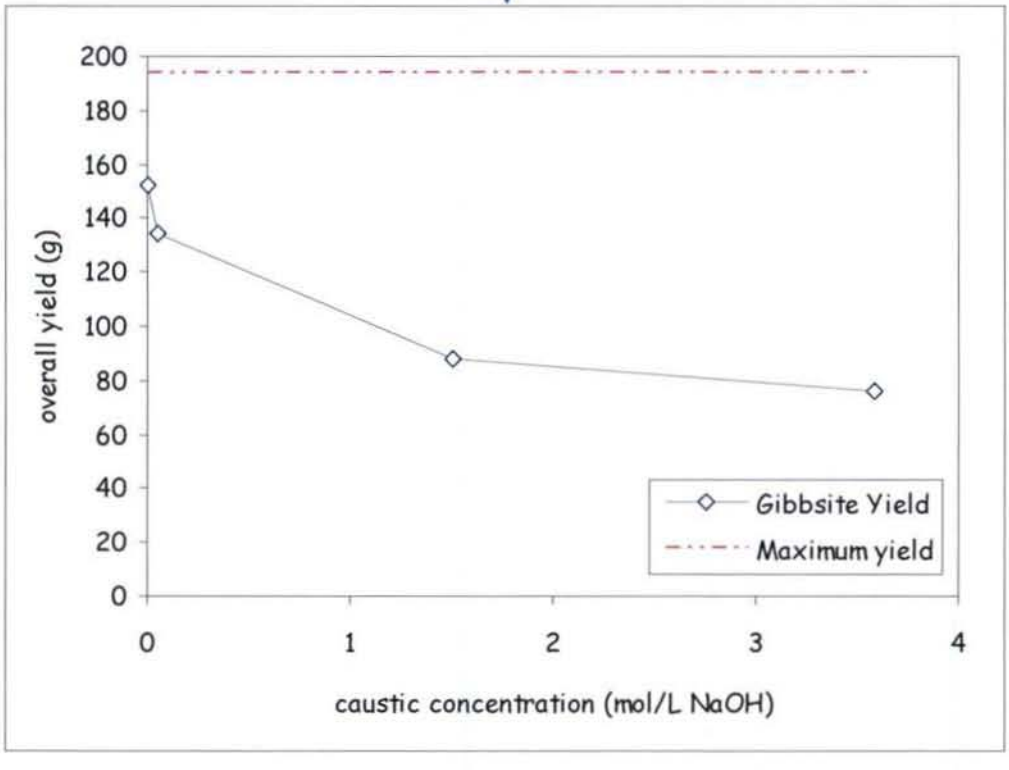
200
180
160
140
120
100
80
60
40
20
0
overall yield (g)
Gibbsite Yield
Maximum yield
0
1
2
3
4
caustic concentration (mol/L NaOH)

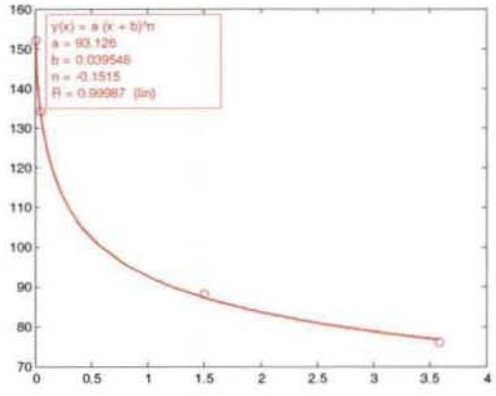

Matlab curve fitting of the overall yield curve with source code:

```
function createfigure(x1, y1, x2, y2)
%CREATEFIGURE(X1,Y1,X2,Y2)
%  X1:  vector of x data
%  Y1:  vector of y data
%  X2:  vector of x data
%  Y2:  vector of y data

%  Auto-generated by MATLAB on 31-Jul-2008 09:54:05

%% Create figure
figure1 = figure('PaperPosition',[0.6345 6.345 20.3
15.23],'PaperSize',[20.98 29.68]);

%% Create axes
axes1 = axes('Parent',figure1);
box(axes1,'on');
hold(axes1,'all');

%% Create plot
plot1 = plot(...
  x1,y1,...
  'Color',[1 0 0],...
  'LineStyle','none',...
  'Marker','o');

%% Create plot
plot2 = plot(x2,y2,'LineWidth',2);

%% Create textbox
annotation1 = annotation(...
  figure1,'textbox',...
  'Position',[0.15 0.6957 0.3 0.2143],...
  'BackgroundColor',[1 1 1],...
  'EdgeColor',[1 0.5 0],...
  'Color',[1 0.5 0],...
  'Margin',3,...
  'String',{'y(x) = a (x + b)\^n','a = 93.126','b = 0.039546','n = -
0.1515','R = 0.99987  (lin)'},...
  'FitHeightToText','on');
```

EXP CODE:	B1	B2	B3	
Time (min)	ppt (g)	ppt (g)	ppt (g)	Abs. max (g)
0	0	0	0	194
15	15	86	40	194
30	41	104	44	194
45	48	110	44	194
60	45	114	48	194
90	64	134	50	194
105	62	140	54	194
120	61	148	58	194
180	73	152	74	194
240	76	152	88	194

EXP CODE:	B4
Time (min)	ppt (g)
0	0
15	12
30	26
45	36
60	46
90	74
105	98
120	120
180	134
240	134

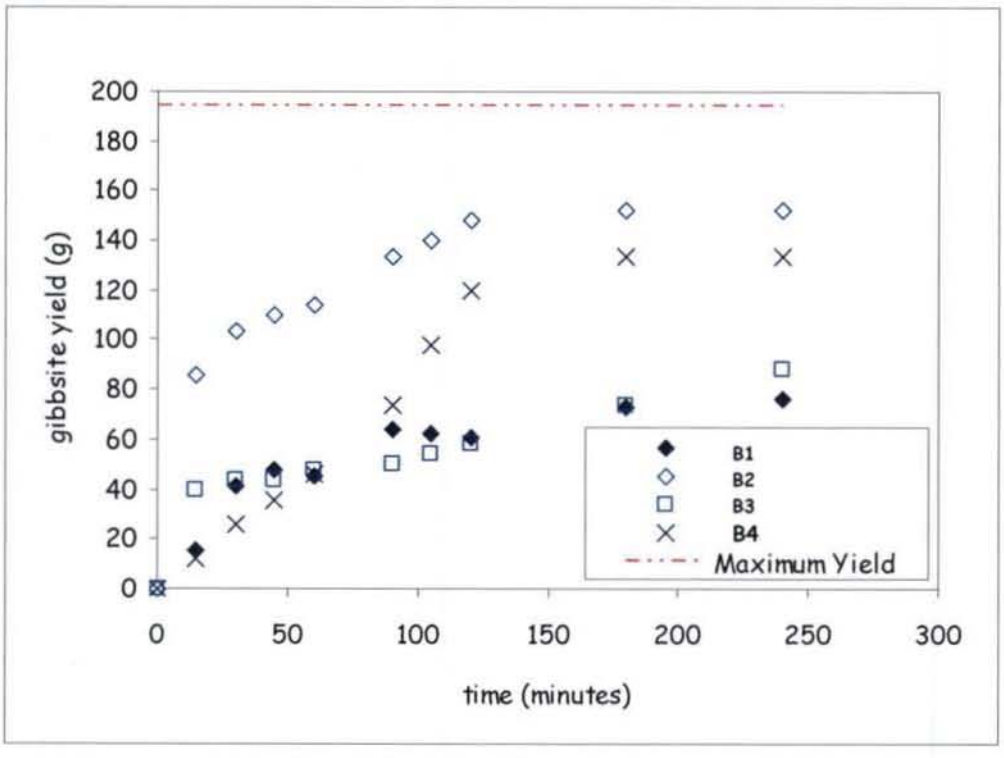

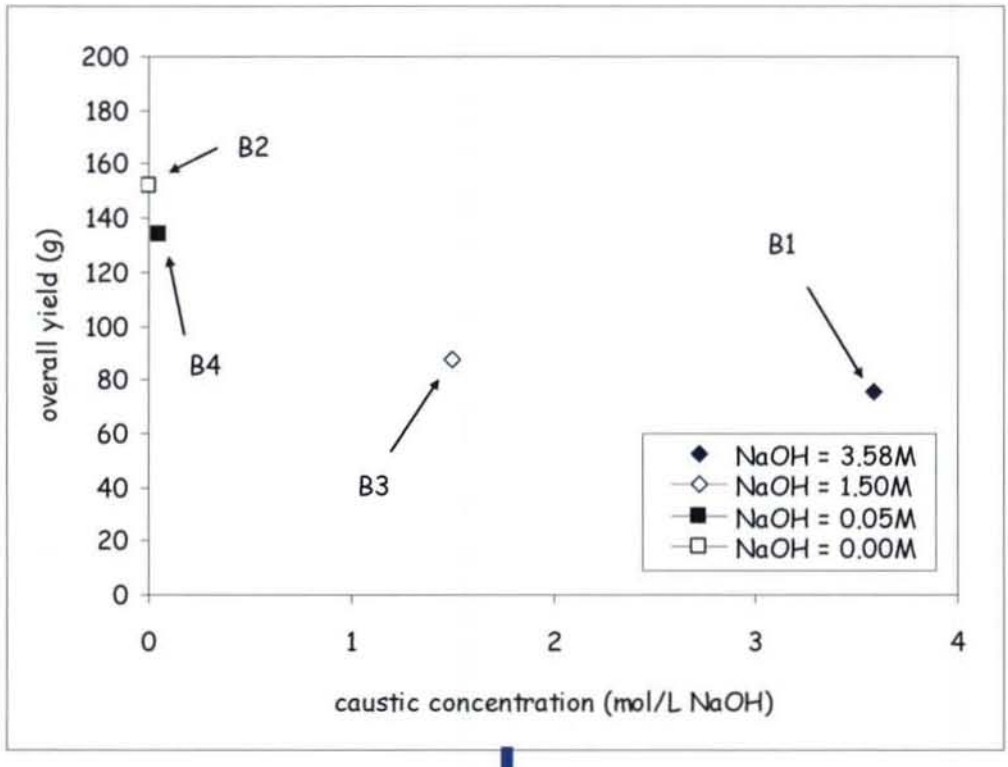
200
180
160
140
120
100
80
60
40
20
0
overall yield (g)
B2
B1
B4
B3
NaOH = 3.58M
NaOH = 1.50M
NaOH = 0.05M
NaOH = 0.00M
0
1
2
3
4
caustic concentration (mol/L NaOH)

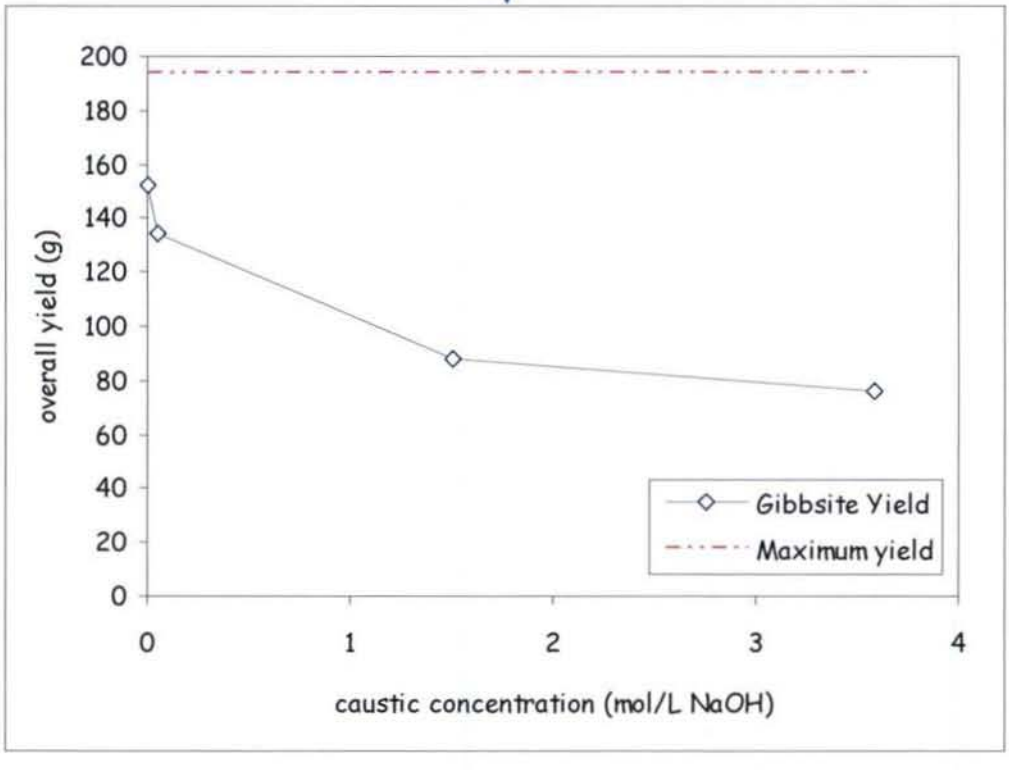
200
180
160
140
120
100
80
60
40
20
0
overall yield (g)
Gibbsite Yield
Maximum yield
0
1
2
3
4
caustic concentration (mol/L NaOH)

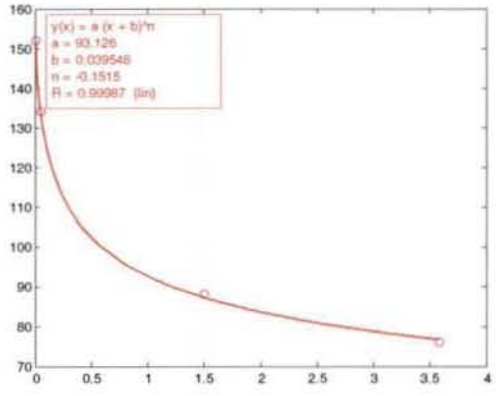

Matlab curve fitting of the overall yield curve with source code:

```
function createfigure(x1, y1, x2, y2)
%CREATEFIGURE(X1,Y1,X2,Y2)
%  X1:  vector of x data
%  Y1:  vector of y data
%  X2:  vector of x data
%  Y2:  vector of y data

%  Auto-generated by MATLAB on 31-Jul-2008 09:54:05

%% Create figure
figure1 = figure('PaperPosition',[0.6345 6.345 20.3
15.23],'PaperSize',[20.98 29.68]);

%% Create axes
axes1 = axes('Parent',figure1);
box(axes1,'on');
hold(axes1,'all');

%% Create plot
plot1 = plot(...
  x1,y1,...
  'Color',[1 0 0],...
  'LineStyle','none',...
  'Marker','o');

%% Create plot
plot2 = plot(x2,y2,'LineWidth',2);

%% Create textbox
annotation1 = annotation(...
  figure1,'textbox',...
  'Position',[0.15 0.6957 0.3 0.2143],...
  'BackgroundColor',[1 1 1],...
  'EdgeColor',[1 0.5 0],...
  'Color',[1 0.5 0],...
  'Margin',3,...
  'String',{'y(x) = a (x + b)\^n','a = 93.126','b = 0.039546','n = -
0.1515','R = 0.99987  (lin)'},...
  'FitHeightToText','on');
```

10.2 Seed loading data

Gibbsite overall yield at different initial seed laodings

EXP CODE:	B5		B6	
Time (min)	ppt (g)	S	ppt (g)	S
0	0.00	3.96	0.00	3.96
15	103.51	3.72	125.20	2.83
30	122.47	2.94	134.17	2.46
45	130.48	2.61	137.09	2.34
60	132.23	2.54	142.98	2.10
75	144.16	2.05	142.00	2.14
90	148.34	1.88	144.38	2.04
105	149.63	1.82	145.38	2.00
120	151.82	1.73	144.53	2.03
180	155.81	1.57	148.23	1.88
240	157.68	1.49	147.18	1.93
Seeding:	50 g/L		100 g/L	

Particle size distribution for experiment B5:

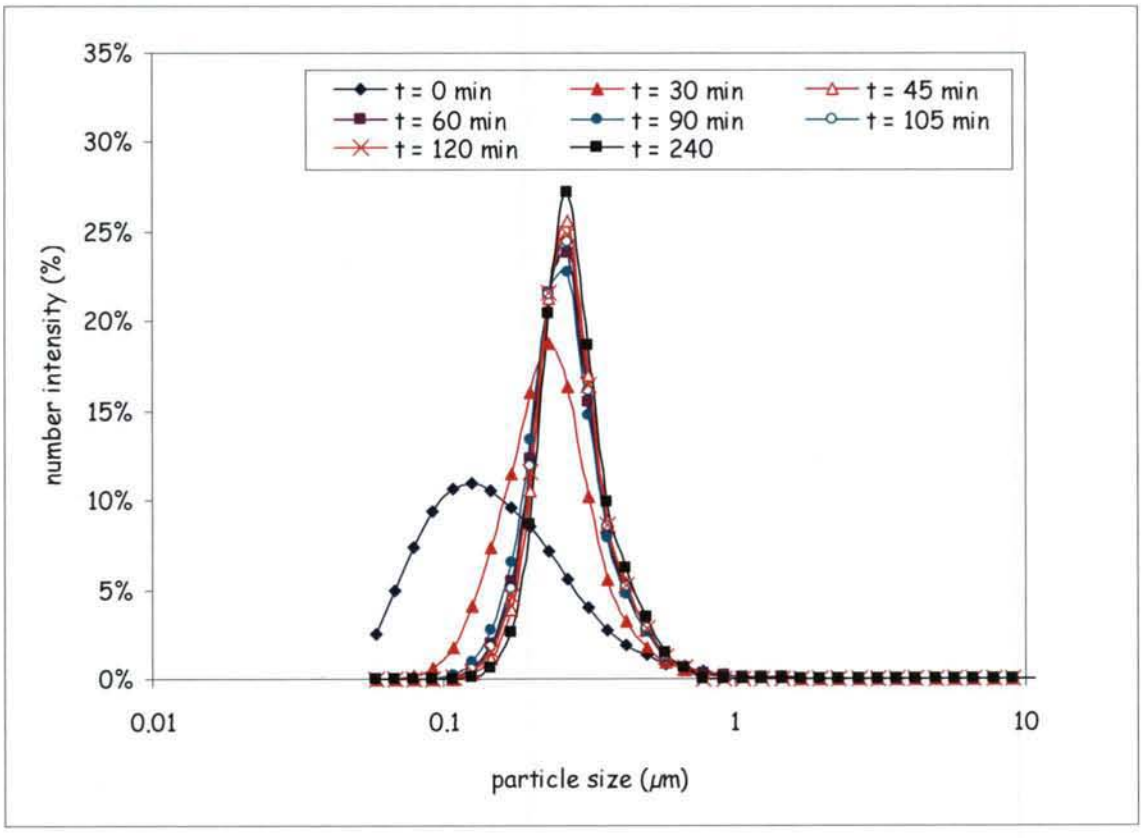

Particle size distribution for experiment B6:

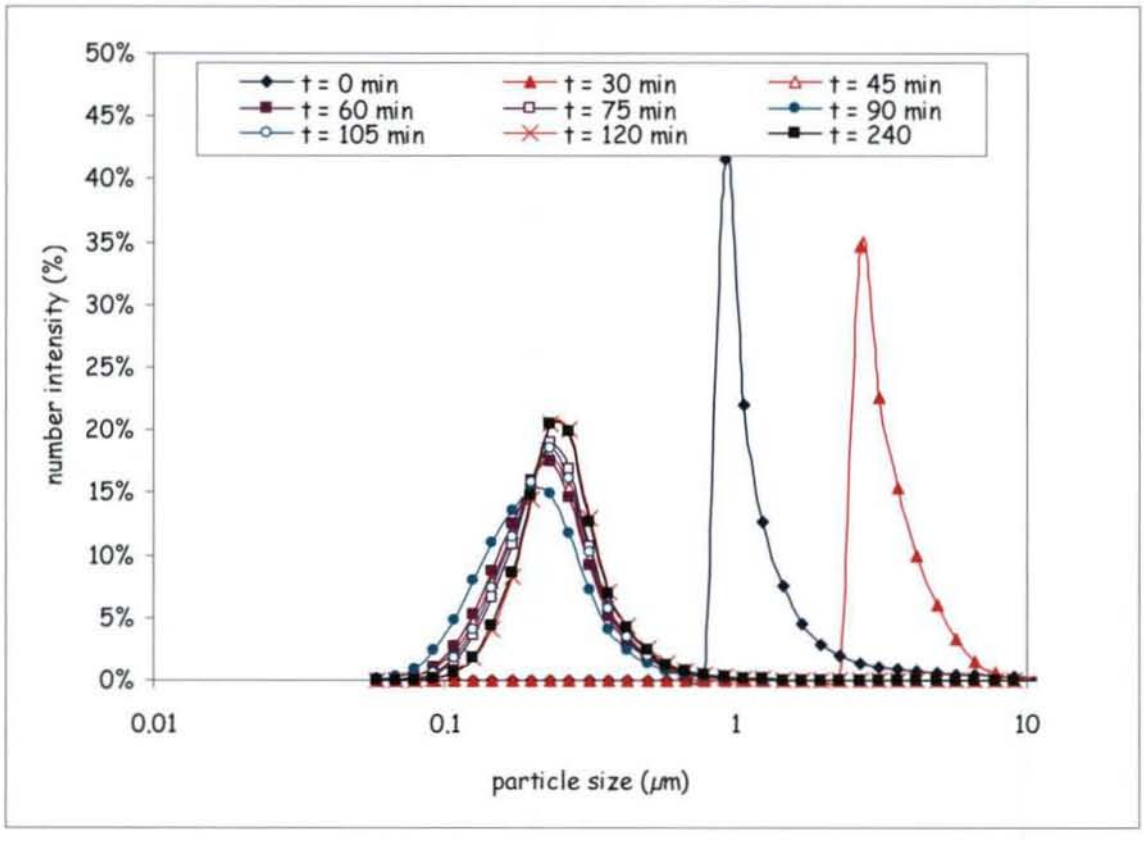

Mathematica script for aggregation and growth extraction (The method of Bramley, Hounslow and Ryall), 1996:

For B5:

```
<<DPB`

file=ToFileName[{$TopDirectory,"AddOns\Applications\DPB\Documentation\English"}
,"BTCH-5.txt"]

 C:\Program Files\Wolfram
Research\Mathematica\5.2\AddOns\Applications\DPB\Documentation\English\BTCH-
5.txt

rawdata=ReadSSFile[file,SizeScaleFactor□10^-6]

data=DeltaNtoN[rawdata]

Getalistofjthmoments[data,0]

{915.492,899.863,1152.63,870.457,853.125,638.705,594.872,552.723,1178.,1049.63}

Getalistofjthmoments[data,1]

{0.0215148,0.0105141,0.0209092,0.00947331,0.0260843,0.0141935,0.0106647,0.00855
182,0.0567752,0.367908}

Getalistofjthmoments[data,2]

\!\({0.00001272967588474699`, 6.777768091501056`*^-7, 1.73146652548464`*^-6, \

5.393473261901531`*^-7, 0.00001542013409432372`, 1.1323444875568668`*^-6, \

7.657130376470029`*^-7, 5.566456056455269`*^-7, 5.554426971315093`*^-6, \

0.00024160236283644556`}\)\

Getalistofjthmoments[data,3]

\!\({9.19991427686536`*^-9, 6.700178096453527`*^-11, \

2.0277392494329286`*^-10, 4.9147479866705556`*^-11,

    1.1151516251702864`*^-8, 1.2708268912051627`*^-10, \

7.960937565942627`*^-11, 5.352490194219715`*^-11, 6.887821022096266`*^-10, \

1.6678975350305795`*^-7}\)
```

```
Getalistofjthmoments[data,4]
\!\({6.790586750076047`*^-12, 7.985099303084062`*^-15, \
2.7961978899617246`*^-14, 5.443315165845496`*^-15, 8.240204366204152`*^-12, \
1.6956252824032986`*^-14, 9.951036742737086`*^-15, 6.203549951170713`*^-15, \
9.848505425166078`*^-14, 1.1901880319524335`*^-10}\)
Getalistofsizes[data]
\!\({5.363006591796865`*^-8, 6.756964895729832`*^-8, 8.513242305530732`*^-8, \
1.072601318359373`*^-7, 1.3513929791459666`*^-7, 1.7026484611061466`*^-7, \
2.145202636718746`*^-7, 2.7027859582919326`*^-7, 3.405296922212294`*^-7, \
4.290405273437494`*^-7, 5.405571916583867`*^-7, 6.810593844424588`*^-7, \
8.580810546874984`*^-7, 1.081114383316773`*^-6, 1.362118768884917`*^-6, \
1.7161621093749968`*^-6, 2.162228766633548`*^-6, 2.7242375377698363`*^-6, \
3.4323242187499966`*^-6, 4.3244575332670964`*^-6, 5.4484750755396726`*^-6, \
6.864648437499993`*^-6, 8.648915066534191`*^-6, 0.00001089695015107 9345`,
    0.000013729296874999974`, 0.00001729783013306837`, \
0.00002179390030215867 3`, 0.00002745859374999995`, 0.00003459566026613674 4`, \
0.00004358780060431735`, 0.00005491718749999999`, 0.00006919132053227348`, \
0.00008717560120863482`, 0.00010983437499999997`, 0.00013838264106454717`, \
0.00017435120241726966`, 0.00021966874999999997`, 0.00027676528212909 44`, \
0.00034870240483453937`, 0.00043933749999999994`, 0.00055353056425818 87`, \
0.00069748096690786`}\)
GetalistofStandardDeviations[data]
{0.000115553,0.000024833,0.0000342507,0.0000223869,0.00013092,0.0000357637,0.\
0000310771,0.0000277076,0.0000489106,0.000327597}
mechanisms={Growth True,Aggregation True};
rates = ExtractRateConstants[data, mechanisms, UseEquations -> {0, 3}]
rates=ExtractRateConstants[data,mechanisms,UseEquations\[Rule]{0,3}]
\!\({Nucleation \[Rule] False,
      Growth \[Rule] True, GrowthRateConstantKnown \[Rule] False,
      GrowthSizeDependence \[Rule] SizeIndependent, GrowthDrivingForce \
```

\[Rule] Time, G0Data \[Rule] {{0.`, \(-1.555026348207532`*^-6\)}, {
      900.`, \(-2.4150719277470025`*^-6\)}, {1800.`, \
\(-1.8760354222967504`*^-9\)}, {2700.`, 3.6932438582705196`*^-6}, {3600.`, \
5.327189380492274`*^-7}, {5400.`, \(-6.006004633569706`*^-7\)}, {6300.`, \
\(-1.7477322235268442`*^-8\)}, {7200.`, 7.121999310087886`*^-9}, {10800.`, \
1.3653468758138246`*^-6}, {14400.`, 2.759007227643986`*^-7}}, Aggregation \
\[Rule] True, AggregationRateConstantKnown \[Rule] False, \
AggregationSizeDependence \[Rule] SizeIndependent, AggregationDrivingForce \
\[Rule] Time, AggregationInnerKernel \[Rule] None, Beta0Data \[Rule] {{0.`, \
4.4408897894276053`*^-7}, {900.`, \(-2.4969693849930165`*^-7\)}, {1800.`, \
4.171383962350781`*^-8}, {2700.`, 3.384216780671379`*^-7}, {3600.`, \
1.2725113786640922`*^-7}, {5400.`, 3.166558749434778`*^-7}, {6300.`,
          2.706181000644842`*^-7}, {7200.`, 1.211906715453343`*^-7}, \
{10800.`, \(-2.3791796689927694`*^-7\)}, {
         14400.`, 1.0394324083892968`*^-7}}, Breakage \[Rule]
           False, Sink \[Rule] False}\)

RateConstantPlot[GrowthRateConstantKnown True,rates,mechanisms]

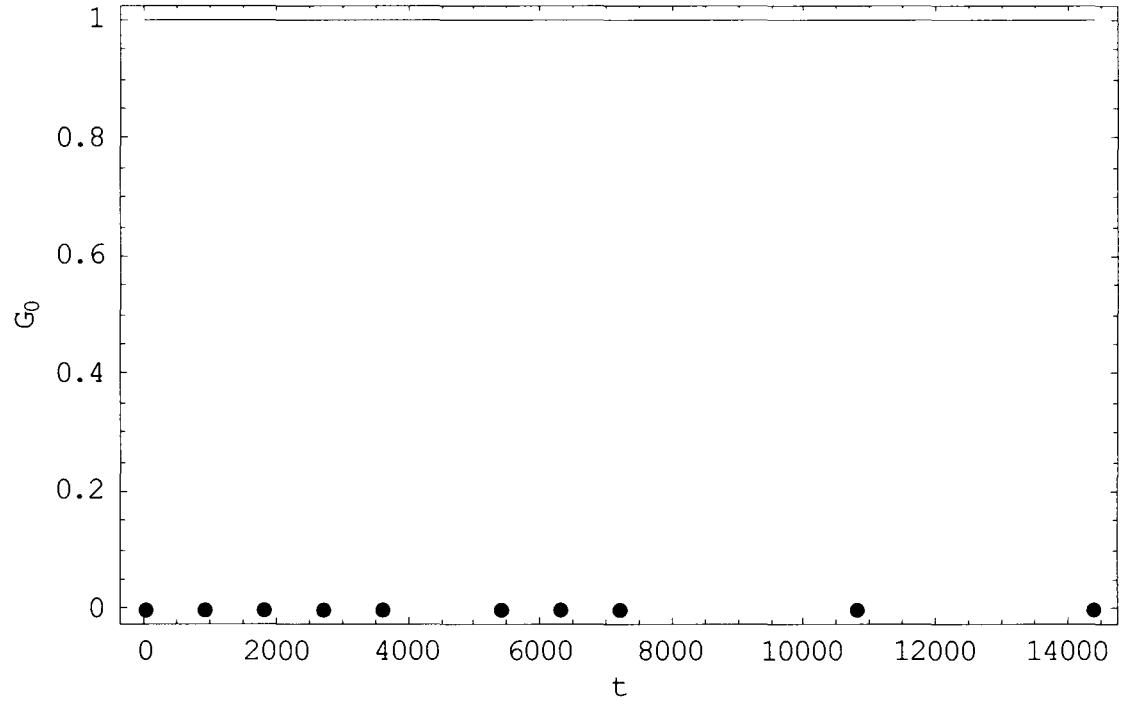

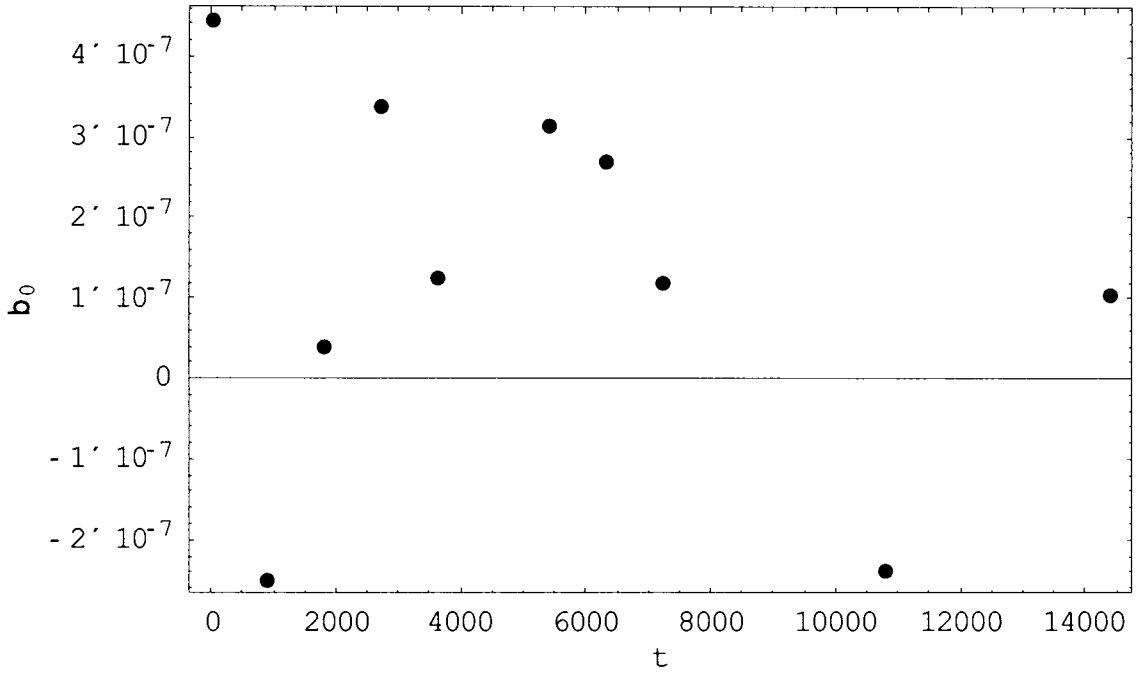

{□Graphics□,□Graphics□}

For B6:

```
<<DPB`
file=ToFileName[{$TopDirectory,"
    AddOns\Applications\DPB\Documentation\English"},"BTCH-6.txt"]
C:\Program Files\Wolfram \
Research\Mathematica\5.2\AddOns\Applications\DPB\Documentation\English\BTCH-6.\
txt
rawdata=ReadSSFile[file,SizeScaleFactor\[Rule]10^-6]
data=DeltaNtoN[rawdata]
Getalistofjthmoments[data,0]
\!\({2.1722021813042493`*^11, 9.835112164598818`*^9, 4.015818966988184`*^10, \
1.786228700733208`*^11, 2.544476933312395`*^11, 2.162918103108795`*^11, \
2.712034849434889`*^11, 3.12552276750375`*^11, 2.455432182736692`*^11, \
2.235913644667785`*^11, 3.0992610994966656`*^11}\)
Getalistofjthmoments[data,1]
\!\({1.9595852620042744`*^6, 442143.18540960667`, 402117.83235947293`, \
447596.4114486688`, 533032.9224518661`, 409105.9981788896`, \
461481.4124969819`, 494486.79262854555`, 427138.54576598504`, \
409277.50206133595`, 439815.0485347955`}\)
Getalistofjthmoments[data,2]
{1036.31,33.2588,25.0374,23.5018,22.2054,20.7228,16.9737,18.4643,14.8897,12.\
4951,11.7012}
Getalistofjthmoments[data,3]
{0.721388,0.00340504,0.00288744,0.00272176,0.00259335,0.00246124,0.0019973,0.\
00218857,0.00174897,0.00147084,0.00137864}
Getalistofjthmoments[data,4]
\!\({0.0005180118255528774`, 4.160562705632494`*^-7, 3.972352066069782`*^-7, \
3.733811964145455`*^-7, 3.615139281728394`*^-7, 3.444438122718975`*^-7, \
2.8113376465858773`*^-7, 3.078587646961919`*^-7, 2.4633074236352653`*^-7, \
2.0864109815531853`*^-7, 1.9553218627928333`*^-7}\)
```

```
Getalistofsizes[data]
\!\({5.363006530761709`*^-8, 6.756964818830353`*^-8, 8.513242208643461`*^-8, \
1.0726013061523418`*^-7, 1.351392963766071`*^-7, 1.7026484417286925`*^-7, \
2.1452026123046836`*^-7, 2.7027859275321413`*^-7, 3.4052968834573855`*^-7, \
4.2904052246093693`*^-7,
    5.405571855064285`*^-7, 6.810593766914771`*^-7, 8.580810449218734`*^-7, \
1.0811143710128565`*^-6, 1.3621187533829538`*^-6, 1.7161620898437469`*^-6, \
2.1622287420257148`*^-6, 2.7242375067659096`*^-6, 3.4323241796874967`*^-6, \
4.32445748405143`*^-6, 5.448475013531819`*^-6, 6.864648359374993`*^-6, \
8.648914968102859`*^-6, 0.00001089695002706 3639`, 0.000013729296718749975`, \
0.000017297829936205704`, 0.00002179390005412726`, 0.00002745859343749995`,
    0.000034595659872411416`, 0.00004358780010825453`,
     0.000054917186874999 9`, 0.00006919131974482282`,
    0.000087175600216509 16`, 0.00010983437374999998`,
    0.000138382639489645 88`, 0.00017435120043301835`,
    0.000219668747499999 98`, 0.00027676527897929176`,
    0.000348702400866036 76`, 0.00043933749499999996`, 0.0005535305579585835`, \
0.0006974048017320734`}\)
mechanisms={Growth\[Rule]True,Aggregation\[Rule]True};
rates=ExtractRateConstants[data,mechanisms,UseEquations\[Rule]{3,4}]
\!\({Nucleation \[Rule] False,
      Growth \[Rule] True, GrowthRateConstantKnown \[Rule] False,
      GrowthSizeDependence \[Rule] SizeIndependent, GrowthDrivingForce \
\[Rule] Time, G0Data \[Rule] {{0.`, \(-1.9036831576686163`*^-7\)}, {
      900.`, \(-3.9303679274880645`*^-6\)}, {1800.`, \
\(-4.964990916822464`*^-9\)}, {2700.`, \(-2.2766479292336875`*^-9\)}, \
{3600.`, \(-2.1345293238567316`*^-9\)}, {4500.`, \(-5.23294097960269`*^-9\)}, \
{5400.`, \(-2.9225816102885388`*^-9\)}, {6300.`, \
\(-2.446841277710845`*^-9\)}, {7200.`, \(-8.9340278394678`*^-9\)}, {10800.`, \
\(-1.3480385358748771`*^-9\)}, {14400.`, 5.976923576406659`*^-12}}, \
```

```
Aggregation \[Rule] True, AggregationRateConstantKnown \[Rule] False,
        AggregationSizeDependence \[Rule] SizeIndependent, \
AggregationDrivingForce \[Rule] Time, AggregationInnerKernel \[Rule] None, \
Beta0Data \[Rule] {{
            0.`, 1.0473039571173928`*^-12}, {900.`, \
\(-8.408904687403839`*^-10\)}, {1800.`, 2.4024559428179665`*^-13}, {

            2700.`, 4.605919443044358`*^-14}, {3600.`, \
6.082475489498437`*^-14}, {4500.`,
          9.079907369008572`*^-14}, {5400.`, 6.196186316483054`*^-14}, \
{6300.`, 3.907739150154936`*^-14}, {7200.`, 1.7172218376810234`*^-13}, \
{10800.`, 3.5395153930933354`*^-14}, {14400.`, \
\(-8.089925614978512`*^-15\)}}, Breakage \[Rule] False, Sink \[Rule] False}\)
```

RateConstantPlot[GrowthRateConstantKnown True,rates,mechanisms]

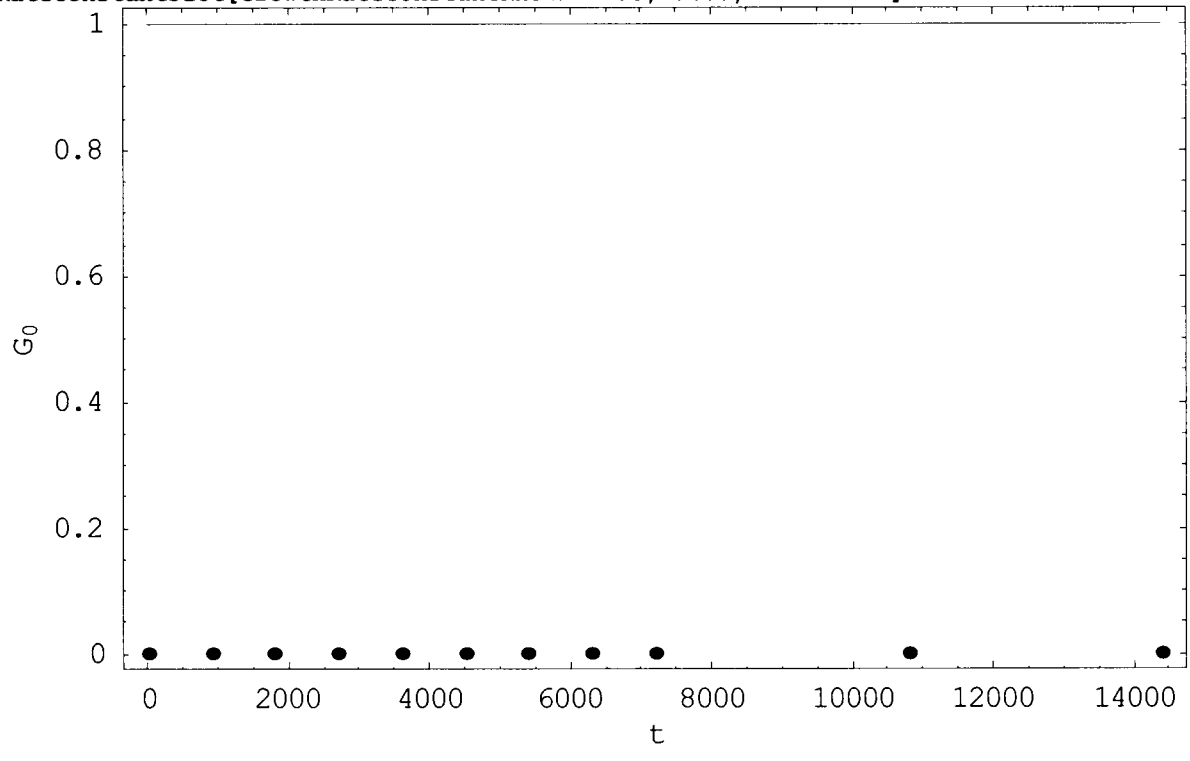

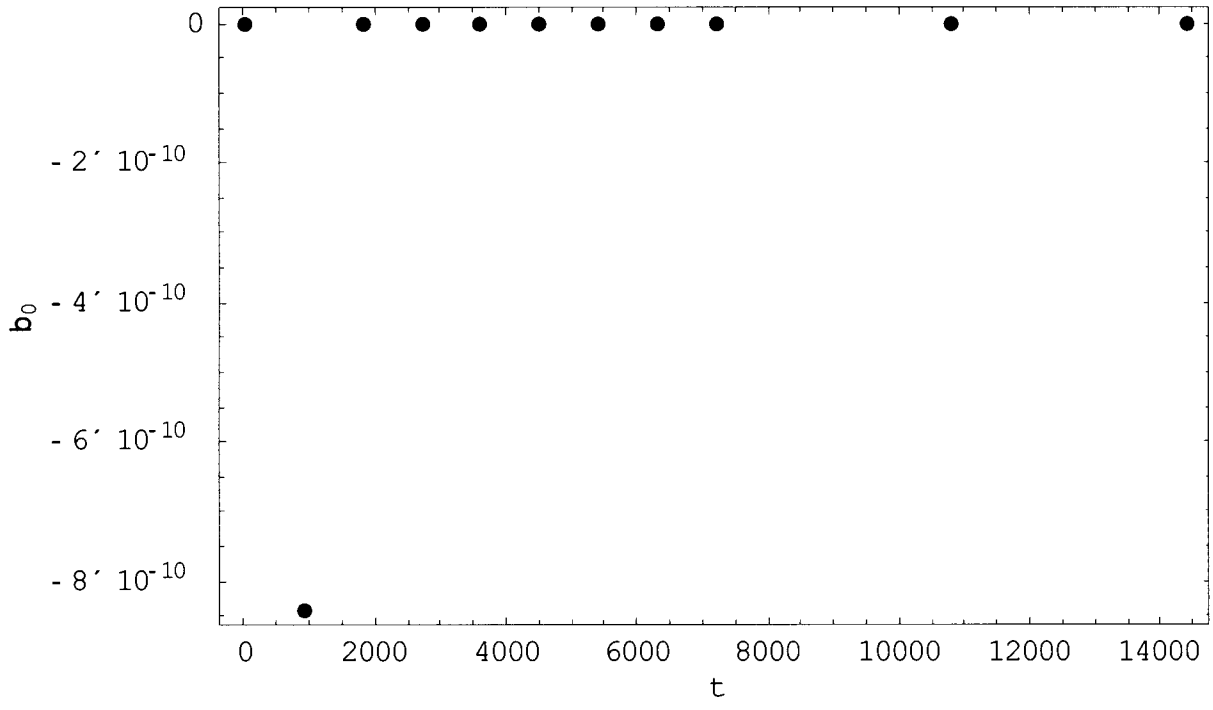

{□Graphics□,□Graphics□}

-

10.3 Pregnant Bayer Liquor Parameter Calculations

Colour codes: input

output

Input Bayer liquor parameter (g/L):

$Gibbsite_{added} := 194$ $NaOH_{added} := 143.4$ $Na2CO3_{added} := 40$ $T := 80$

Resultant composition (g/L):

$$A := \frac{Gibbsite_{added}}{2\cdot[\,26.981 + 3\cdot(15.9994 + 1.007)\,]}\cdot[\,2\cdot(26.981) + 3\cdot(15.9994)\,]$$

$A = 126.796$ in g/L of Al_2O_3

$$TC := \frac{NaOH_{added}}{2\cdot(22.989 + 15.9994 + 1.007)}\cdot[\,2(22.989) + 12.0107 + 3(15.9994)\,]$$

$TC = 190.003$ in g/L of Na_2CO_3

$TA := TC + Na2CO3_{added}$

$TA = 230.003$ in g/L of Na_2CO_3

Pregnant liquor feed ratios:

$\frac{A}{TC} = 0.667$ initial alumina/caustic ratio

$\frac{TC}{TA} = 0.826$ industrial feed causticisation efficiency

---

10.4 Effect of antisolvent on the gibbsite equilibrium solubility

$V_{initial} := 1$ {initial liquor volume in L}

$V_{added} := 1$ {antisolvent added in L}

$c_{added} := 0$ {NaOH concentration within the antisolvent in mol/L}

$V_{reactor} := V_{initial} + V_{added}$ {total liquor volume after addition in L}

$$C := \frac{TC \cdot V_{initial} + c_{added} \cdot V_{added}}{V_{reactor}}$$

precipitation NaOH concentration mol/L using a mole balance

Total ionic strength (g/L):

$I := 0.01887 \cdot C + 0.01911 \cdot Na2CO3_{added}$

$I = 2.557$ ionic strength in g/Na_2CO_3

Equilibrium solubility (g/L):

$\Delta G := -30960$ Gibbs free energy of dissolution in J/mol

$R := 8.314$ Ideal gas constant in J/mol/K

$$A_{eqm} := 0.96197 \cdot C \cdot \left[1 + \frac{10^{\left[\frac{-9.2082 \cdot \sqrt{I}}{(1+\sqrt{I})} + 0.8743 \cdot I - 0.2149 \cdot I^{\frac{3}{2}} \right]}}{\exp\left[\frac{\Delta G}{R \cdot (273 + T)} \right]} \right]^{-1}$$

$A_{eqm} = 31.787$ Equilibrium solubility in gAl_2O_3

Bayer supersaturations:

$$S := \frac{A}{A_{eqm}}$$ $S = 3.989$ in ratio form

$$S := \frac{A - A_{eqm}}{A_{eqm}}$$ $S = 2.989$ in relative form

$$S := \frac{A - A_{eqm}}{C}$$ $S = 1$ in absolute form

10.5 Mixing and minimum impeller speed calculations

Colour codes: input

output

Input reactor configurations:

$V_{slurry} := 2000$ reactor slurry load: ml

$T_{reactor} := 128.75$ vessel inner diameter: mm

$$H := \frac{10V_{slurry}}{\pi\left(\frac{T_{reactor}}{20}\right)^2}$$ $H = 153.619$ slurry height: mm

$C := 27.90$ impeller bottom clearance: mm

$D := 45.00$ impeller diameter: mm

Aspect ratio:

$$R := \frac{H}{T_{reactor}}$$ $R = 1.193$ aspect ratio must be < 2.5 for systems with solid suspensi

an aspect ratio of < 1.3 was used to negate the need for multiple impellers to be used on a single shaft

---

Clearance ratio and the nondimensional parameter:

$\frac{C}{T} = 0.349$ clearance ratio < 0.25 using 45°C pitch-blade impeller

$$S := 2.28\left(\frac{T}{D}\right)^{0.83}\exp\left[0.65\left(\frac{C}{T}\right)\right]$$ $S = 4.611$ nondimensional parameter for a batch system using a 45° pitch-blade impeller with a clearance ratio of < 0.25

Minimum impeller speed for particle suspension:

$g := 9.81$ gravitational acceleration in m/s^2

$d_{particle} := 25 \cdot 10^{-6}$ mean particle size in m

$\rho_{solid} := 2.42$ gibbsite density in kg/m^3

$d_{particle} := 45 \cdot 10^{-6}$ mean particle size in m

$$I := \frac{I}{2 \cdot (22.989) + 12.0107 + 3 \cdot (15.9994)}$$ $I = 0.024$ ionic strength conversion to mol/kg

Solving for liquor density at 70°C with feed A/C ratio (double interpolation):

$\rho_{70°C} := 1.2$ initial guess

Given

$$\frac{\frac{A}{TC} - 0.577}{\rho_{70°C} - 1.133358} = \frac{0.481 - 0.577}{1.127027 - 1.133358}$$

$\rho_{70°C} := \text{Find}(\rho_{70°C})$ $\rho_{70°C} = 1.139$

Solving for liquor density at 90°C with feed A/C ratio (double interpolation):

$\rho_{90°C} := 1.2$ initial guess

Given

$$\frac{\frac{A}{TC} - 0.385}{\rho_{90°C} - 1.10125} = \frac{0.289 - 0.385}{1.09315 - 1.10125}$$

$\rho_{90°C} := \text{Find}(\rho_{90°C})$ $\rho_{90°C} = 1.125$

Solving for liquor density at 80°C with feed A/C ratio (double interpolation):

$\rho_{80°C} := 1.2$ initial guess

Given

$$\frac{\rho_{80°C} - \rho_{90°C}}{T - 90} = \frac{\rho_{70°C} - \rho_{90°C}}{70 - 90}$$

$\rho_{80°C} := \text{Find}(\rho_{90°C})$ $\rho_{80°C} = 1.261$

$\rho_{liquor} := \rho_{80°C}$ Bayer liquor density at 80°C in kg/m^3 determined via a double linear interpolation using experimental data obtained from Königsberger et al. (2005)

$V_{total\_liquor} := 2000$ input solid-free Bayer liquor loading: ml

$M_{solid} := 50$ seed loading: grams per litre liquor

$M_{liquor} := \rho_{liquor} \cdot V_{total\_liquor}$ $M_{liquor} = 2521.4$ solid-free liquor mass: grams

$X := \frac{M_{solid}}{M_{liquor}}$ $X = 0.02$ solid-to-liquor mass ratio determined experimentally

$\nu := 400$ kinematic viscosity: m^2/s

$$N_{js} := S \cdot \nu^{0.1} \left[\frac{g \cdot (\rho_{solid} - \rho_{liquor})}{\rho_{liquor}} \right]^{0.45} \frac{d_{particle}}{\left(\frac{D}{1000} \right)^{0.85}} X^{0.13}$$

$N_{js} = 8.521 \times 10^{-3}$ impeller speed: RPS

Suspension cloud height due to agitation:

$H_{cloud} := \frac{H}{1000}$ set cloud height equal to liquor level: m

$N_{op} := 100$ initial guess for operating agitation speed: RPS

Given

$$H_{cloud} = \frac{N_{op}}{N_{js}}\left[0.84 - 1.05\frac{C}{T_{reactor}} + 0.7\frac{\left(\frac{D}{T_{reactor}}\right)^2}{1-\left(\frac{D}{T_{reactor}}\right)^2}\right]$$

$N_{op} := \text{Find}(N_{op})$ $N_{op} = 1.844 \times 10^{-3}$

10.6 Reactor design assembly diagrams